Table 3 Number of peaks detected from human urine with sheathless and sheath-flow methods

	Sheath-flow				Sheathless			
	Sample A	Sample B	Sample C	Average	Sample A	Sample B	Sample C	Average
Total	2039	1328	1609	1659	18 796	16 268	13 378	16 147
$3 < S/N \leqq 10$	1231	826	962	1006	12 606	12 395	9624	11 542
$10 < S/N \leqq 100$	732	449	594	592	5547	3510	3408	4155
$100 < S/N$	76	53	53	61	643	363	346	451

γ-Glutamylcysteine and γ-glutamyl-2-aminobutyrate were synthesized at the Toray Research Center (Tokyo, Japan). All other reagents were obtained from Wako Pure Chemicals Industries Ltd. (Osaka, Japan). All chemicals used were of analytical or reagent grade. Stock solutions (1–100 mmol L^{-1}) were prepared in either Milli-Q (Millipore, Billerica, MA) water, aqueous 0.1 mol L^{-1} HCl, or aqueous 0.1 mol L^{-1} NaOH. The working mixture standard was prepared by diluting these stock solutions with Milli-Q water just before analysis.

Sample preparation

Urine samples were collected from a healthy volunteer. An aliquot (20 μL) of the urine sample was placed in a tube and mixed with 20 μL of an aqueous solution of methionine sulfone (2 mmol L^{-1}) and 3-aminopyrrolidine (2 mmol L^{-1}), and 160 μL of Milli-Q water. The solution was then centrifugally filtered through a 5 kDa cutoff filter (Millipore) to remove proteins. The filtrate was used for subsequent CE- time-of-flight mass spectrometry (TOFMS).

Instrumentation

The sheathless CE-TOFMS experiments were carried out with a PA 800 *plus* capillary electrophoresis system (Beckman Coulter) and an Agilent 6220 Accurate-Mass TOF LC/MS system (Agilent Technologies, Palo Alto, CA).

The sheath-flow CE-TOFMS experiments were performed using an Agilent CE capillary electrophoresis system equipped with an Agilent 6220 Accurate-Mass TOF LC/MS system, an Agilent 1100 series isocratic HPLC pump, an Agilent CE-MS adapter kit, and an Agilent CE-ESI-MS sprayer kit (Agilent Technologies).

Sheathless CE-TOFMS conditions

A prototype HSPS (fused-silica, 30 μm i.d., 150 μm o.d., 90 cm total length) with a porous segment (approximately 3 cm) on its outlet terminal was supplied by Beckman Coulter (Fig. 7). The HSPS capillary was inserted into a stainless steel ESI needle to enable electrical contact between the electrolyte and conductive liquid *via* a secondary capillary (fused-silica, 50 μm i.d., 360 μm o.d., 80 cm total length). A nanospray end cap and a gas diverter were installed instead of the standard ESI end cap.

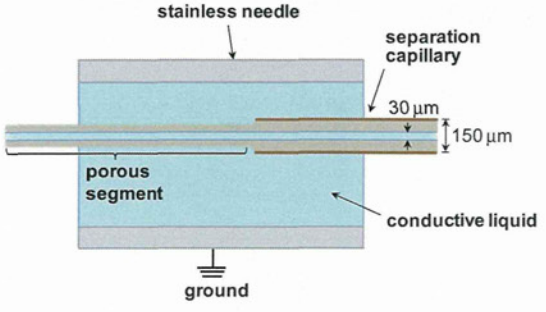

Fig. 7 Schematic representation for the high-sensitivity porous sprayer interface.

Before use, the new capillary was successively flushed at 345 kPa with methanol (5 min), Milli-Q water (5 min), 0.1 mol L^{-1} hydrochloric acid (5 min), Milli-Q water (5 min), 1 mol L^{-1} sodium hydroxide (30 min), Milli-Q water (5 min) and BGE (5 min). The HSPS was then placed on a *xyz* stage, and the position of the tip was optimized by maximizing the signals for three reference compounds (leucine, tryptophan and guanosine) under continuous electrophoresis.

Aqueous acetic acid (10% v/v, pH 2.2) was used as the BGE and conductive liquid. Between runs, the capillary was flushed with the BGE for 5 min at 345 kPa, and then the stainless steel ESI needle was refilled with conductive liquid for 0.5 min at 345 kPa. The sample solution (2.6 nL) was injected at 20.7 kPa for 5 s. A constant separation voltage of 25 kV was applied after it was increased from 0 to 25 kV over the first minute of the analysis. The capillary was maintained at room temperature (25 °C), and the sample tray was cooled to 10 °C.

ESI-TOFMS was conducted in positive ion mode and the capillary voltage was set at a value between 850 and 950 V, which depended on the distance between the porous tip and the MS inlet. For TOFMS, the optimized fragmentor voltage, skimmer voltage, and octupole radio frequency voltage (Oct RFV) were 200 V, 75 V, and 250 V, respectively. An automatic recalibration function was performed using the following two reference masses: an ammonium adduct ion of acetic acid, $(CH_3COOH + NH_4)^+$, *m/z* 78.05493; and protonated di-sec-octyl phthalate, $(C_{24}H_{38}O_4 + H)^+$, *m/z* 391.28429. Exact mass data were acquired at a rate of 1.5 spectra per second from *m/z* 50 to 1000.

Sheath-flow CE-TOFMS conditions

Conventional sheath-flow CE-MS was carried out as previously described.[9,28] Briefly, samples were separated in a fused-silica capillary (50 μm i.d., 360 μm o.d., 100 cm total length) filled with either 1 mol L^{-1} formic acid or 10% (v/v) aqueous acetic acid (pH 2.2) as the BGE. The sample solution was injected at 5 kPa for 3 s (2.3 nL) and a positive voltage of 30 kV was applied. The temperatures of the capillary and the sample tray were maintained at 20 °C and 5 °C, respectively. The sheath liquid was methanol–water (50% v/v) containing 0.1 μmol L^{-1} hexakis with a flow rate of 10 μL min^{-1}.

ESI-TOFMS was operated in positive ion mode and the capillary voltage was set at 4 kV. A capillary gas (dry nitrogen)

heated to 300 °C was used at a flow rate of 7 L min^{-1}. In TOFMS, the fragmentor voltage, skimmer voltage and Oct RFV were set at 75, 50 and 125 V, respectively. Automatic recalibration of each acquired spectrum was performed using the masses of the following reference standards: ^{13}C isotopic ion of protonated methanol dimer, $(2CH_3OH + H)^+$, *m/z* 66.06306; and $(hexakis + H)^+$, *m/z* 622.02896. Exact mass data were acquired at 1.5 spectra per second from *m/z* 50 to 1000.

Data analysis

The acquired raw CE-TOFMS data were analyzed using our proprietary software for quantitation of metabolites.[11] Peak identification was performed by matching the *m/z* values and normalized migration times with those of standard reagents.

Conclusions

A sheathless CE-MS with a HSPS capillary was evaluated for the analysis of cationic metabolites. Satisfactory resolution was achieved for validation of compounds using 10% aqueous acetic acid as the BGE. The method had good reproducibility, linearity and sensitivity, which allowed detection of cationic metabolites at levels of several femtomoles or lower. Compared with conventional sheath-flow CE-MS, although a decrease in sensitivity was observed for some metabolites, the sheathless approach increased the sensitivity by more than 5-fold for 40% of the metabolites analyzed. The method was applied to the analysis of cationic metabolites in human urine. The number of peaks detected was 10 times that with conventional methods, and more than 180 successive runs were conducted without any problems. These results indicate that the proposed sheathless CE-MS method is promising for metabolome analysis of cationic species in many areas.

Acknowledgements

We thank John C. Hudson, Lena Sripitisawad, Jean-Marc Busnel, Jerald S. Feitelson, and Etsuo Arai (Beckman Coulter, Inc) for providing the HSPS sprayer interface and technical support. We also thank Dr Cheng Kian Kai (Institute for Advanced Biosciences, Keio University) for critical reading of the manuscript. This work was supported financially by the Yamagata Prefectural Government and the City of Tsuruoka.

References

1 H. L. Chuang, Y. T. Huang, C. C. Chiu, C. D. Liao, F. L. Hsu, C. C. Huang and C. C. Hou, *J. Nutr. Biochem.*, 2012, **23**, 752–758.
2 M. Ooi, S. Nishiumi, T. Yoshie, Y. Shiomi, M. Kohashi, K. Fukunaga, S. Nakamura, T. Matsumoto, N. Hatano and M. Shinohara, *Inflammation Res.*, 2011, 1–10.
3 S. U. Bajad, W. Lu, E. H. Kimball, J. Yuan, C. Peterson and J. D. Rabinowitz, *J. Chromatogr., A*, 2006, **1125**, 76–88.
4 P. Bernini, I. Bertini, C. Luchinat, L. Tenori and A. Tognaccini, *J. Proteome Res.*, 2011, **10**, 4983–4992.
5 W. C. Yang, F. E. Regnier and J. Adamec, *Electrophoresis*, 2008, **29**, 4549–4560.
6 T. Soga, Y. Ueno, H. Naraoka, Y. Ohashi, M. Tomita and T. Nishioka, *Anal. Chem.*, 2002, **74**, 2233–2239.
7 T. Soga, Y. Ohashi, Y. Ueno, H. Naraoka, M. Tomita and T. Nishioka, *J. Proteome Res.*, 2003, **2**, 488–494.
8 T. Soga, R. Baran, M. Suematsu, Y. Ueno, S. Ikeda, T. Sakurakawa, Y. Kakazu, T. Ishikawa, M. Robert, T. Nishioka and M. Tomita, *J. Biol. Chem.*, 2006, **281**, 16768–16776.
9 A. Hirayama, K. Kami, M. Sugimoto, M. Sugawara, N. Toki, H. Onozuka, T. Kinoshita, N. Saito, A. Ochiai, M. Tomita, H. Esumi and T. Soga, *Cancer Res.*, 2009, **69**, 4918–4925.
10 T. Soga, K. Igarashi, C. Ito, K. Mizobuchi, H. P. Zimmermann and M. Tomita, *Anal. Chem.*, 2009, **81**, 6165–6174.
11 M. Sugimoto, D. T. Wong, A. Hirayama, T. Soga and M. Tomita, *Metabolomics*, 2010, **6**, 78–95.
12 T. Soga, M. Sugimoto, M. Honma, M. Mori, K. Igarashi, K. Kashikura, S. Ikeda, A. Hirayama, T. Yamamoto, H. Yoshida, M. Otsuka, S. Tsuji, Y. Yatomi, T. Sakuragawa, H. Watanabe, K. Nihei, T. Saito, S. Kawata, H. Suzuki, M. Tomita and M. Suematsu, *J. Hepatol.*, 2011, **55**, 896–905.
13 M. Moini, *Anal. Bioanal. Chem.*, 2002, **373**, 466–480.
14 Z. Kele, G. Ferenc, E. Klement, G. K. Toth and T. Janaky, *Rapid Commun. Mass Spectrom.*, 2005, **19**, 881–885.
15 M. S. Kriger, K. D. Cook and R. S. Ramsey, *Anal. Chem.*, 1995, **67**, 385–389.
16 Y. R. Chen and G. R. Her, *Rapid Commun. Mass Spectrom.*, 2003, **17**, 437–441.
17 A. D. Zamfir, N. Dinca, E. Sisu and J. Peter-Katalinic, *J. Sep. Sci.*, 2006, **29**, 414–422.
18 V. Sanz-Nebot, E. Balaguer, F. Benavente and J. Barbosa, *Electrophoresis*, 2005, **26**, 1457–1465.
19 P. Cao and M. Moini, *J. Am. Soc. Mass Spectrom.*, 1997, **8**, 561–564.
20 Z. Chen, B. Boggess and H. C. Chang, *J. Mass Spectrom.*, 2007, **42**, 244–253.
21 L. H. Shi, Y. X. Jin, D. C. Moon, S. K. Kim and S. R. Park, *Electrophoresis*, 2009, **30**, 1661–1669.
22 M. Moini, *Anal. Chem.*, 2007, **79**, 4241–4246.
23 J. M. Busnel, B. Schoenmaker, R. Ramautar, A. Carrasco-Pancorbo, C. Ratnayake, J. S. Feitelson, J. D. Chapman, A. M. Deelder and O. A. Mayboroda, *Anal. Chem.*, 2010, **82**, 9476–9483.
24 K. Faserl, B. Sarg, L. Kremser and H. Lindner, *Anal. Chem.*, 2011, **83**, 7297–7305.
25 R. Haselberg, C. K. Ratnayake, G. J. de Jong and G. W. Somsen, *J. Chromatogr., A*, 2010, **1217**, 7605–7611.
26 M. Kawai, Y. Iwamuro, R. Iio-Ishimaru, S. Chinaka, N. Takayama and K. Hayakawa, *Anal. Sci.*, 2011, **27**, 857–860.
27 R. Ramautar, J. M. Busnel, A. M. Deelder and O. A. Mayboroda, *Anal. Chem.*, 2012, **84**, 885–892.
28 T. Soga and D. N. Heiger, *Anal. Chem.*, 2000, **72**, 1236–1241.
29 J. Samskog, M. Wetterhall, S. Jacobsson and K. Markides, *J. Mass Spectrom.*, 2000, **35**, 919–924.

International Journal of Cardiology 161 (2012) 130–136

Contents lists available at ScienceDirect

International Journal of Cardiology

journal homepage: www.elsevier.com/locate/ijcard

Analysis of liver metabolism in a rat model of heart failure ☆

Takao Kato [a,b], Shinichiro Niizuma [a], Yasutaka Inuzuka [a], Tsuneaki Kawashima [a], Junji Okuda [a], Akira Kawamoto [a], Yodo Tamaki [a], Yoshitaka Iwanaga [a], Tomoyoshi Soga [c], Toru Kita [a], Takeshi Kimura [a], Tetsuo Shioi [a,*]

[a] Department of Cardiovascular Medicine, Graduate School of Medicine, Kyoto University, Kyoto, Japan
[b] Division of Cardiology, The Tazuke Kofukai Medical Reseach Institute, Kitano Hospital, Osaka, Japan
[c] Institute for Advanced Bioscience, Keio University, Yamagata, Japan

ARTICLE INFO

Article history:
Received 28 December 2010
Received in revised form 5 July 2011
Accepted 10 July 2011
Available online 11 August 2011

Keywords:
Heart failure
Cachexia
Liver
Lipogenesis
Inflammation

ABSTRACT

Background: Cachexia, namely body wasting, is a common complication in cases of congestive heart failure (CHF). Although, neurohumoral and immune abnormalities are associated with the condition, precisely how the imbalance of catabolism and anabolism is responsible for the wasting process is not known.
Methods: We analyzed markers of cachexia in Dahl salt-sensitive rats which show marked hypertension with preserved systolic function at 11 weeks and CHF at 17–19 weeks of age. We also analyzed the change in hepatic metabolism associated with CHF since liver plays a central role in the systemic regulation of catabolism and anabolism.
Results: In CHF rats, a failure to grow was observed and blood hepatic protein levels were decreased associated with increased blood proinflammatory cytokine levels, indicating that Dahl rats serve as a model of cardiac cachexia. Food intake was reduced, and blood sugar and insulin levels were decreased. Despite the apparent fasting condition, blood fatty acid levels were decreased and triglycerides levels were increased. In CHF rats, liver incorporated more glucose, the gene expression related to gluconeogenesis was decreased, the gene expression related to lipogenesis was increased, and the triglyceride content of the liver was increased. The paradoxical production of triglycerides synthesis in fasting rats was associated with a proinflammatory response in liver.
Conclusions: The Dahl salt-sensitive rat can be used as a model of cardiac cachexia. The cachexia was associated with abnormal hepatic metabolism that might work as a maladaptive response during the progression of CHF.

1. Introduction

Congestive heart failure (CHF) is becoming a serious health care problem. CHF is associated with a significant change in energy metabolism of the heart, and the altered energetics is hypothesized to play an important role in the progression of CHF [1]. Using a Dahl rat model which shows a distinct transition from compensated left ventricular hypertrophy to CHF, we recently found that left ventricular hypertrophy or CHF was associated with a distinct change in the metabolic profile of the heart and that the metabolic remodeling of heart might be a therapeutic target [2].

CHF is also associated with abnormal energy metabolism in extra-cardiac tissues. Cachexia, namely body wasting, is a common complication among CHF patients [3,4]. Cardiac cachexia is associated with a poor prognosis and disability. Several lines of evidence suggest that neurohumoral and immune abnormalities play a critical role, and a complex imbalance of catabolism and anabolism is likely to be responsible for the development of the wasting process [4].

Although cardiac cachexia is an important complication and a potential target of therapeutic intervention in cases of CHF, its pathophysiology is poorly understood. One reason for this is the limited number of animal models of cardiac cachexia available. There is a report that the skeletal muscle atrophy caused by reduced activity is significantly different from the muscle atrophy observed in CHF rats [5]. However, the mechanism by which the imbalance between catabolism and anabolism is induced is not clear. In this study, we have shown that the Dahl salt-sensitive rat fed a high-salt diet is an animal model of cardiac cachexia. To gain insight into the mechanism of cardiac cachexia, we have analyzed the change of hepatic

☆ Grant support: Grants from the Japan Society for the Promotion of Science, Japan Heart Foundation, Japan Foundation of Cardiovascular Research, NOVARTIS Foundation for the Promotion of Science, Mochida Memorial Foundation for Medical and Pharmaceutical Research, Takeda Science Foundation, and Vehicle Racing Commemorative Foundation.

* Corresponding author at: Department of Cardiovascular Medicine, Graduate School of Medicine, Kyoto University, 54 Shogoinkawahara-cho, Sakyo-ku, Kyoto 606-8507, Japan. Tel.: +81 75 751 3670; fax: +81 75 751 3203.
E-mail address: tshioi@kuhp.kyoto-u.ac.jp (T. Shioi).

0167-5273/$ – see front matter © 2011 Elsevier Ireland Ltd. All rights reserved.
doi:10.1016/j.ijcard.2011.07.056

Table 1
Primer sequences used in real time quantitative RT-PCR.

Gene	Forward	Reverse	Ref.	GenBank entry
18SrRNA	AGTCCCTGCCCTTTGTACACA	CGATCCGAGGGCCTCACTA	[26]	M11188
Pyruvate carboxylase	CCGTTCTAAGGTGCTAAAGGA	GACGAGTATTCAGGCTATCCA		BC085680.1
Phosphoenolpyruvate carboxykinase (PEPCK)	ATGTCAGAAGAGGACTTCGAGA	CTCAATACCAATCTTGGCCAGA		BC085680.1
ATP Citrate lyase	GGCAAGATCCTCATCATTGGA	CAACTTCTCCCATCACTCGTA		BC100618.1
Acetyl-CoA carboxylase (ACC) α	ATGATTGCTGGGGAATCCTCA	GAGGTGTATACTTCCCGACCA		NM_022193.1
Fatty acid synthase	CAAGTTATTCGACCACCCAGA	TCACCCAGTTGTCTTTCCAGA		NM_017332.1
Sterol regulatory element-binding protein (SREBP) 1c	TCACTGAAAGACCTGGTGTCA	GCTTTCACCTGGTTATCCTCA		AF286470.2
Sterol regulatory element-binding protein (SREBP) 2	CAAGTACCTGCAGCAGGTCA	AGTCAATGGAATAGGGGGAGA		NM_001033694
Tumor necrosis factor (TNF)α	ATGGTCCTCTTTCAGTCG GAG	TGTC TACTGAACTTCGGGGTG	[27]	NM_012675.3
Interleukin (IL)1β	CTTCCCCAGGACATGCTAGG	CAAAGGCTTCCCCTGGAGAC	[28]	NM_031512.2
C-reactive protein (CRP)	ACATTGTGGGGACAAATGCA	ACATTGGGGCTGAATACCCTA		NM_017096.3
Transthyretin	GGCTCACCACAGATGAGAAGTTC	ACAAATGGGAGCTACTGCTTTGGC	[29]	NM_012681.1
Retinol-binding protein (RBP) 4	AGAAGGGTCATATGAGCGCTA	GTATCGATGATCCAGTGGTCA		NM_013162.1
Hepatocyte nuclear factor (HNF) 4	AAATGTGCAGGTGTTGACCA	CACGCTCCTCCTGAAGAATC	[29]	EF193392

metabolism since the liver plays a central role in the systemic regulation of catabolism and anabolism.

2. Materials and methods

2.1. Animals

Inbred male Dahl salt-sensitive (DS) rats (Japan SLC, Hamamatsu, Shizuoka, Japan) were fed a 0.3% NaCl (low salt; LS) diet until the age of 6 weeks, then an 8% NaCl (high salt; HS) diet [2]. DS rats fed only the low-salt diet were used as controls. Animal care and the experiments were approved by the Institutional Animal Care and Use Committee of Kyoto University and conducted by the Guide for the Care and Use of Laboratory Animals published by the United States National Institutes of Health.

2.2. Protocols

Serial measurements of body weight, food intake, and cardiac function by echocardiography were performed from 11 weeks of age. Blood samples were obtained at age 18 weeks without fasting. The measurement of mRNAs, proteins, and metabolites was performed at the age of 11 and 18 weeks without fasting. The hepatic uptake of ^{18}F-deoxyglucose (FDG) and ^{125}I-15-(*p*-iodophenyl)-9-*R,S*-methylpentadecanoic acid (9MPA) was measured at age 11 and 18 weeks after an overnight fast.

2.3. Cardiac echocardiography

Echocardiography was performed based on a previously reported protocol [2]. Briefly, rats were anesthetized with inhaled diethyl ether (Wako Pure Chemical Industries, Osaka, Japan), and transthoracic echocardiography was performed using a Sonos-5500 echocardiograph (Agilent Technologies, Santa Clara, CA) with a 15-MHz linear transducer. M-mode echocardiograms were obtained at the papillary muscle level. At least two independent M-mode measurements for each animal were carried out.

2.4. Blood analysis

Blood samples were collected without fasting via the right ventricle, and the samples were centrifuged at 3000 rpm for 15 min and analyzed as described [2]. Plasma concentration of insulin was analyzed using a commercial kit (Shibayagi Co., Shibukawa, Gunma, Japan).

2.5. Sampling of hepatic tissue

To obtain liver tissues for biochemical analyses, 11-week-old LS (n = 6), 11-week-old HS (n = 8), and 17-week-old HS (n = 6) rats were sacrificed by decapitation without fasting. A piece of the liver was obtained from the right lobe, rapidly divided, snap frozen in liquid nitrogen, and stored at −80 °C. The liver tissues were also used for the measurement of mRNA, glycogen, and triglyceride (TG).

2.6. Metabolome analysis (CE-TOFMS)

A targeted metabolomic approach was performed using capillary electrophoresis time-of-flight mass spectrometry (CE-TOFMS) [6]. Hepatic tissue from 11-week-old LS (n = 6), 11-week-old HS (n = 6), and 17-week-old HS (n = 6) rats were analyzed. The conditions used were described in Supplementary materials.

2.7. Levels of glycogen and triglycerides

Glycogen and TGs were extracted from liver tissue of 11-week-old LS, 11-week-old HS, and 17-week-old HS rats (n = 6–8 in each group) using previously described methods [7,8], and analyzed with commercial kits (BioAssay Systems, Hayward, CA, and Cayman Chemical, Ann Arbor, MI, respectively).

2.8. Quantitative reverse transcription-polymerase chain reaction (RT-PCR)

Total RNA was isolated from the liver tissue (n = 6–8 in each group) by the acid guanidinium thiocyanate–phenol–chloroform method. Quantitative RT-PCR was carried out as described previously [2]. The sequences of primers used are listed in Table 1. The mRNA level of each gene was standardized with the corresponding 18S ribosomal RNA as an internal control. The Genbank accession numbers are also included in Table 1.

2.9. Western blotting

Liver lysate was obtained by homogenization in ice-cold buffer [10% glycerol, 137 mM NaCl, 20 mM Tris–HCl pH 7.4, 4 g/ml aprotinin, 4 g/ml leupeptin, 1 mM phenylmethylsulfonyl fluoride (PMSF), 4 g/ml pepstatin, 20 mM NaF, 1 mM sodium pyrophosphate, and 1 mM orthovanadate] [9]. The lysate was kept on ice for 15 min and cleared by centrifugation at 15,000 g for 20 min at 4 °C. Protein concentrations were determined by the Bradford method (BioRad, Hercules, CA). 200 μg of liver tissue lysate was subjected to sodium dodecyl sulfate-polyacrylamide gel electrophoresis (SDS-PAGE), and the proteins were transferred onto polyvinylidene difluoride membranes. The primary antibodies used for western blotting were for sterol regulatory element-binding protein (SREBP) 1 (2A4, 1:500, Santa Cruz, Santa Cruz, CA), SREBP2

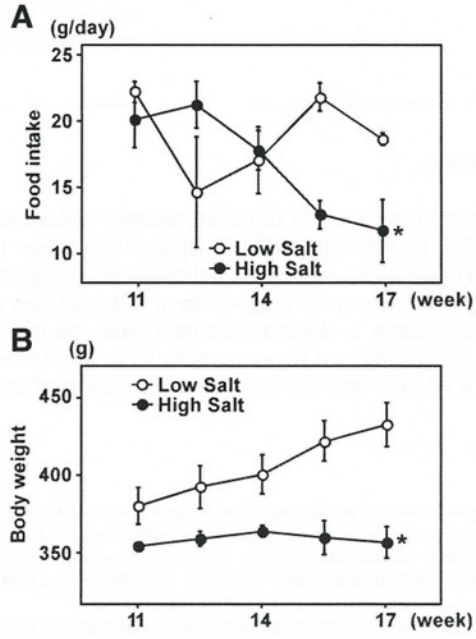

Fig. 1. Food intake and body weight of Dahl rats fed a high-salt diet. (A) Serial measurements of food intake. Rats with congestive heart failure (CHF) ate less than control rats. (B) Serial measurements of body weight. CHF rats showed a failure to grow. n = 4 for each group. *p < 0.05 versus control rats, namely Dahl rats fed a low-salt diet.

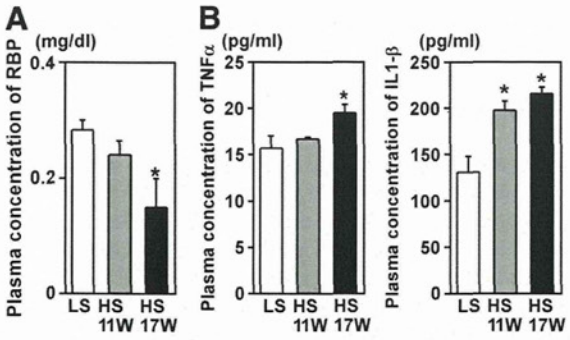

Fig. 2. Markers of cachexia in Dahl rats. (A) The concentration of retinol-binding protein (RBP) in plasma was decreased in CHF rats (HS 17W). (B) The plasma concentration of tumor necrosis factor (TNF)-α and interleukin (IL)1-β was increased in CHF rats. n = 6–8 in each group. LS; low salt, HS; high salt. *p<0.05 versus control LS rats.

(1:500, (Cayman Chemical), and glyceraldehyde-3-phosphate dehydrogenase (GAPDH; 1:1000, Chemicon, Temecula, CA).

2.10. Hepatic uptake of ^{18}FDG and ^{125}I-9MPA

The hepatic uptake of glucose and fatty acids was estimated by measuring the incorporation of an analog of glucose (deoxyglucose) and a fatty acid (9MPA) as described [2]. The 11-week-old LS (n = 7), 11-week-old HS (n = 10), and 17-week-old HS rats (n = 12) were injected with 1 mCi of ^{18}FDG and 20 μCi of ^{125}I-9MPA. The animals were fasted overnight before the injection since variation in the uptake of the isotope-labeled molecule was found when fed animals were used. The rats were sacrificed by decapitation 45 min after the injection, and the livers were removed and washed in cold saline. Specimens of the left lobe were collected and frozen in liquid nitrogen and radioisotopic activity was measured using a scintillation counter (Packard Cobra2 ™ Auto-gamma, GMI, Ramsey, Minnesota) [2]. To measure ^{18}FDG uptake, radioisotopic activity was measured just after sacrifice because the half decay time of ^{18}FDG is 110 min. To measure ^{125}I-9MPA uptake, another radioisotopic measurement was made 48 h after the first. The amount of radioisotope incorporated was presented as a percentage of the administered dose corrected by liver weight in grams. Using this method, cross-talk between the two tracers was negligible [2].

2.11. Plasma and tissue concentrations of inflammatory cytokines

The levels of tumor necrosis factor (TNF)-α and interleukin (IL)1-β in tissue homogenate and plasma were measured using sandwich enzyme-linked immunosorbent assay (ELISA) kits (Shibayagi Co. and R&D Systems; Minneapolis, MN), according to the manufacturers' instructions. The tissue homogenate for the protein analysis was used in this assay.

2.12. Statistical analysis

Values are expressed as means ± SEMs. Differences among experimental groups were tested by ANOVA with post hoc comparisons using the Bonferroni test. In all tests, a value of $p<0.05$ was considered significant.

3. Results

3.1. Dahl rats fed a high-salt diet develop hypertension, heart failure, and cachexia

As we reported previously, DS rats fed a high-salt (HS) diet developed hypertension (HT) at 11 weeks of age (systolic blood pressure; 211 ± 12 mm Hg, diastolic blood pressure; 160 ± 6 mm Hg) [2]. On echocardiographic examination, fractional shortening (FS) was

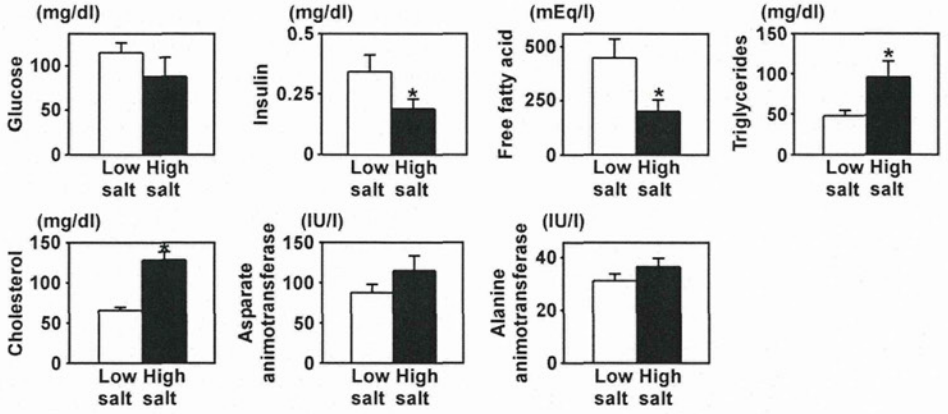

Fig. 3. Blood analysis of Dahl rats. Blood sugar and insulin levels were decreased, and triglyceride and cholesterol levels were increased in CHF rats. n = 5–6 in each group. *p<0.05 versus control rats.

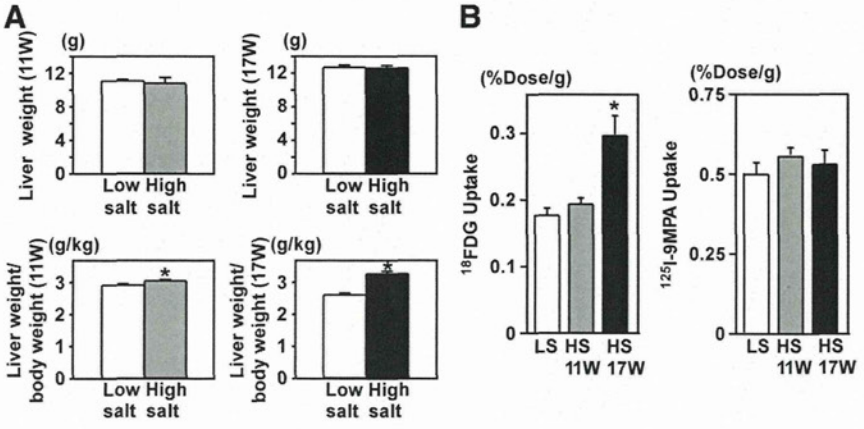

Fig. 4. Liver weight and the uptake of glucose and fatty acids. (A) Liver weight and liver weight corrected by body weight at 11 and 17 weeks of age. Liver weight corrected by body weight was increased in CHF rats (HS 17W) compared with control rats. n = 6–12 in each group. LS; low salt, HS; high salt. *p<0.05 versus control rats. (B) The uptake of ^{18}FDG, a glucose analog, was increased in CHF rats (HS 17W) compared to control rats. The uptake of ^{125}I-9MPA, a fatty acid analog, in the liver was not changed. n = 7–12 in each group. *p<0.05 versus control rats.

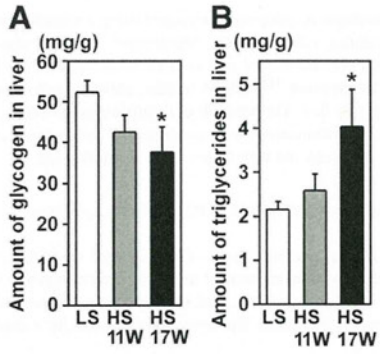

Fig. 5. Glycogen and triglyceride content in liver. (A) The amount of glycogen in liver was decreased in CHF rats. (B) The amount of triglycerides in liver was increased in CHF rats. n = 6–8 in each group. LS; low salt, HS; high salt. *p<0.05 versus control rats.

found to be preserved (62.4 ± 0.9%). At around 17 weeks of age, the rats showed signs of CHF, such as tachypnea and immobilization, and decreased FS (39.7 ± 1.5%). DS rats fed a low-salt (LS) diet did not develop hypertension or CHF, and were used as controls.

Serial measurements of food intake and body weight showed that CHF rats ate less than controls (Fig. 1A) and had a lower body weight (Fig. 1B). The failure to grow in the CHF rats led us hypothesize that the animals may serve as a model of cardiac cachexia. Blood levels of hepatic proteins, such as albumin, transthyretin, and transferrin, can serve as markers of a nutritional index to screen for malnutrition and monitor the metabolic response to dietary intervention [10,11]. Blood hepatic proteins are synthesized mainly in liver and have short half lives in blood. We measured the concentration of retinol-binding protein (RBP), a blood hepatic protein, in plasma and found that it was decreased in CHF rats (Fig. 2A). Cachexia is also known to be associated with neurohumoral and immune abnormalities [4]. Indeed, plasma concentrations of two representative proinflammatory cytokines, TNF-α and IL-1β, were elevated in CHF rats (Fig. 2B).

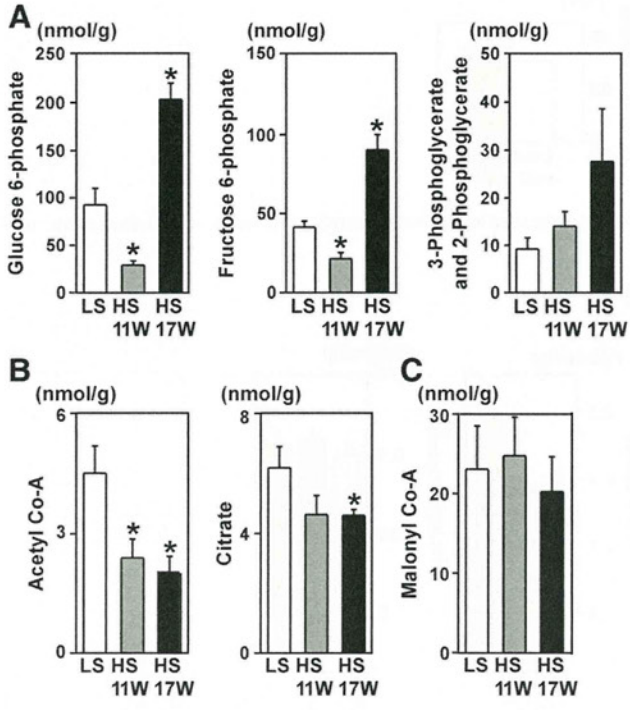

Fig. 6. The amounts of metabolites in liver determined by metabolome analysis. (A) Concentrations of metabolites of glycolysis. (B) Concentrations of metabolites in the Krebs cycle. (C) Malonyl CoA concentration. n = 6 in each group. LS; low salt, HS; high salt. *p<0.05 versus control rats.

3.2. Blood analysis of CHF rats

To investigate the systemic metabolic profile of Dahl rats, we examined blood chemistry. Both glucose and insulin levels were lower in CHF rats than control rats in the fed condition (Fig. 3), as reported [2]. Plasma levels of cholesterol and TG were increased, and free fatty acids (FFAs) were decreased in DS rats with CHF, as reported [2]. Concentrations of representative liver enzymes, such as aspartate amino transferase and alanine transaminase, did not differ among the groups. Lower food intake, associated with lower glucose and insulin levels, suggested that the animals were starved. However, the plasma level of FFAs was decreased and that of TG increased, which is not consistent with a starved condition. Based on these observations, we sought to examine the hepatic metabolism in this model since the liver plays a key role in the homeostasis of systemic catabolism and anabolism.

3.3. Analysis of energy metabolic pathways in the liver

Liver weight corrected by body weight was increased in CHF rats compared with control rats (Fig. 4A). The increase in liver weight is likely to be due to congestion since venous dilation in liver tissue is reported in this model [12]. It is of interest that increased right atrial pressure is reported to indicate malnutrition in CHF patients [13]. Despite lower blood sugar levels, the uptake of ^{18}FDG increased in CHF rats (Fig. 4B). The uptake of ^{125}I-9MPA, a fatty acid analog, was not changed (Fig. 4B). The amount of glycogen in liver was decreased, and that of TG was increased in the CHF rats (Fig. 5A, B). The metabolome analysis (Supplementary table) revealed that levels of some metabolites of glycolysis increased (Fig. 6A) and some metabolites in the Krebs cycle, such as acetyl-CoA and citrate, were decreased (Fig. 6B). Overall, these results may suggest hepatic lipogenesis to be increased and acetyl-CoA to be used for the synthesis of TG and cholesterol.

Next, we examined the gene expression related to lipogenesis and gluconeogenesis. The gene expression of enzymes related to lipogenesis, such as ATP citrate lyase, acetyl-CoA carboxylase, and fatty acid synthase, was up-regulated in CHF rats (Fig. 7A). In contrast, the expression of rate-limiting enzymes in gluconeogenesis, such as pyruvate carboxylase and phosphoenolpyruvate carboxykinase (PEPCK), was down-regulated. Next, we examine the expression of sterol regulatory element-binding protein (SREBP1)1-c and SREBP2, which increase lipogenesis and suppress gluconeogenesis [14,15]. The gene expression of SREBP1-c and SREBP2 was increased in CHF rats. The amount of SERBP proteins was also increased (Fig. 7B and C).

3.4. Expression of rapid turnover protein in liver

Since RBP, a blood hepatic protein, was decreased in the blood of CHF rats, we examined the gene expression of serum hepatic proteins. mRNA levels of transthyretin and retinol-binding protein (RBP) 4 were decreased in CHF rats (Fig. 8A). To examine the mechanism responsible for the decrease of rapid turnover proteins, we measured the expression of hepatocyte nuclear factor (HNF) 4. HNF4 is known to regulate transthyretin gene expression [16,17]. HNF4 mRNA levels started to decrease in rats with HT, and decreased significantly in rats with CHF (Fig. 8B).

3.5. Expression of proinflammatory genes

Inflammatory responses are reported to enhance lipogenesis [18] and induce cachexia [19]. It is well established that CHF is associated with the inflammation of cardiac and extra-cardiac tissue [20]. Thus, local inflammatory responses might be a mechanism causing

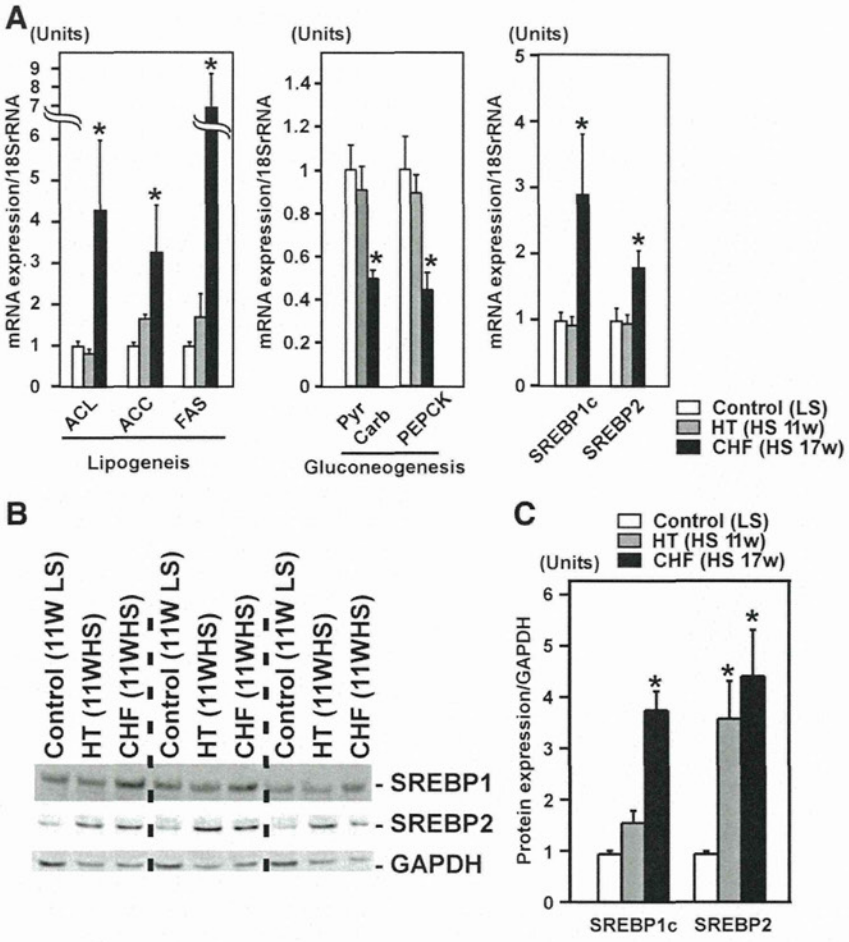

Fig. 7. Expression of mRNA and protein levels related to lipogenesis and gluconeogenesis. (A) The gene expression related to lipogenesis was increased in liver of CHF rats (HS 17W). The gene expression related to gluconeogenesis was decreased. The gene expression of sterol regulatory element-binding protein (SREBP)1c and SREBP2 was increased. n = 6–8 in each group. *p<0.05 versus control rats. (B) Representative images of the Western blotting of SREBP1 and SREBP2. (C) The protein levels of SREBP1 and SREBP2 in liver tissue were increased. n = 3 in each group. LS; low salt, HS; high salt. *p<0.05 versus control rats.

increased lipogenesis and the decreased synthesis of blood hepatic proteins. Therefore, we examined the expression of genes related to proinflammatory responses. The gene expression of TNF-α, IL1-β, and C-reactive protein, started to increase in liver of rats with HT but not with CHF, and significantly increased in CHF (Fig. 9A). The protein levels of TNF-α and interleukin1-β in liver also started to increase in HT rats, and remained increased in CHF rats (Fig. 9B).

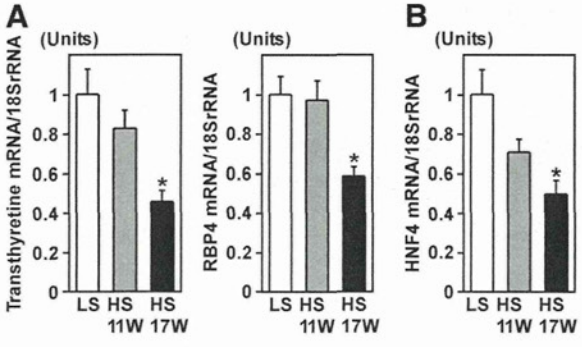

Fig. 8. Analysis of gene expression of hepatic proteins. (A) The gene expression of hepatic proteins, transthyretin and RBP4, was decreased in CHF rats (HS 17W). (B) Hepatocyte nuclear factor (HNF) 4 mRNA was decreased in CHF rats. n = 6–8 in each group. LS; low salt, HS; high salt. *p<0.05 versus control rats.

4. Discussion

In this study, we have shown that Dahl rat fed a high-salt diet developed CHF associated with a failure to grow, decreased blood hepatic protein, and increased blood proinflammatory cytokines. These results indicate the Dahl rat with CHF to be a model of cardiac cachexia.

4.1. Abnormal lipid metabolism in liver of CHF rats

During fasting, liver metabolism changes from anabolism to catabolism. Glucose is produced from glycogen breakdown and gluconeogenesis, and lipid accumulated as TG is used to produce FFAs. The glucose and FFAs are released into the circulation and delivered to the brain, skeletal muscle, the heart etc. However, despite decreased food intake and lower blood sugar and insulin levels, lipogenesis was increased in the liver of CHF rats (Fig. 10). The mechanism by which lipogenesis is increased on fasting in these rats is unknown. However, Fon Tacer et al. reported that giving TNF-α to fasted mice changed the metabolic profile of the liver from lipid usage to synthesis [18]. In that report, SREBP levels were are decreased in fasted mice, but increased on addition of TNF-α, associated with increased lipogenesis. Another report also showed abnormal lipid metabolism to be associated with inflammatory responses in liver [21]. Indeed, SREBPs increased in association with the amount of TNF-α mRNA and protein in this study. The TNF-α concentration in

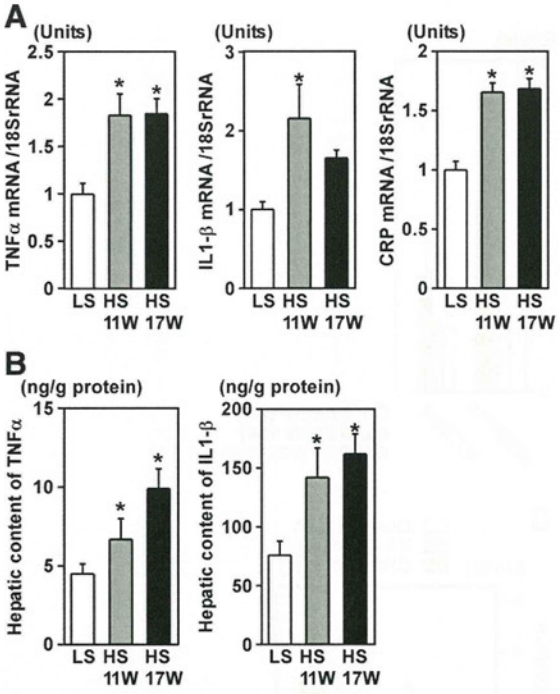

Fig. 9. Expression of proinflammatory cytokines in liver. (A) The gene expression of proinflammatory cytokines, TNF-α, IL1-β, and C-reactive protein (CRP), was increased in HT (HS 11W) and CHF rats (HS 17W). n = 6–8 in each group. (B) The amounts of TNF-α and IL1-β started to increase in the liver in HT rats, and remained increased in the liver in CHF rats assessed by ELISA. n = 6 in each group. LS; low salt, HS; high salt. *p<0.05 versus control rats.

liver was reported to be increased in an animal model of pacing-induced heart failure [22]. Thus, CHF-associated proinflammatory responses may be a mechanism of abnormal lipid metabolism in CHF rats.

4.2. Abnormal blood hepatic protein synthesis in CHF

Blood levels of hepatic proteins are used to evaluate nutritional status, but they are also influenced by many factors other factors. Particularly, the presence of inflammation is known to inversely correlate with circulating levels of hepatic proteins. Indeed, the gene expression of hepatic proteins was decreased associated with local increases in proinflammatory molecules of the liver in this study. However, the mechanism by which inflammation affects hepatic protein is not known [10]. HNF4 regulates the gene expression of transthyretin [16,17]. Although the mechanism by which proinflammatory molecules act on HNF4 expression is unclear, increased levels of SREBPs are known to repress HNF4 gene expression [23].

4.3. Measurement of metabolites using metabolome analysis

The measurement of metabolites in glycolysis and the Krebs cycle provides a snap shot of metabolism. However, based on the findings that ^{18}FDG uptake was increased, the amount of metabolites in glycolysis was increased, the amount of metabolites in the Krebs cycle was decreased, and the TG content was increased, we speculate that acetyl-CoA might be used for *de novo* lipogenesis. Further analysis, in which isotope-labeled glucose or fatty acid is injected and isotope-labeled metabolites are measured, is needed to know how glucose or fatty acids are used to test if the speculation is correct [24,25].

4.4. Potential role of abnormal liver metabolism in cardiac cachexia

Food intake was reduced and blood sugar levels were decreased in this model. During fasting, the liver is expected to deliver energy substrates, such as glucose and FFAs, to peripheral tissues. However, paradoxically, liver incorporated more glucose, the expression of genes related to gluconeogenesis was decreased, the expression of genes related to lipogenesis was increased, and TG content was increased. The response appears to be maladaptive, when the body is

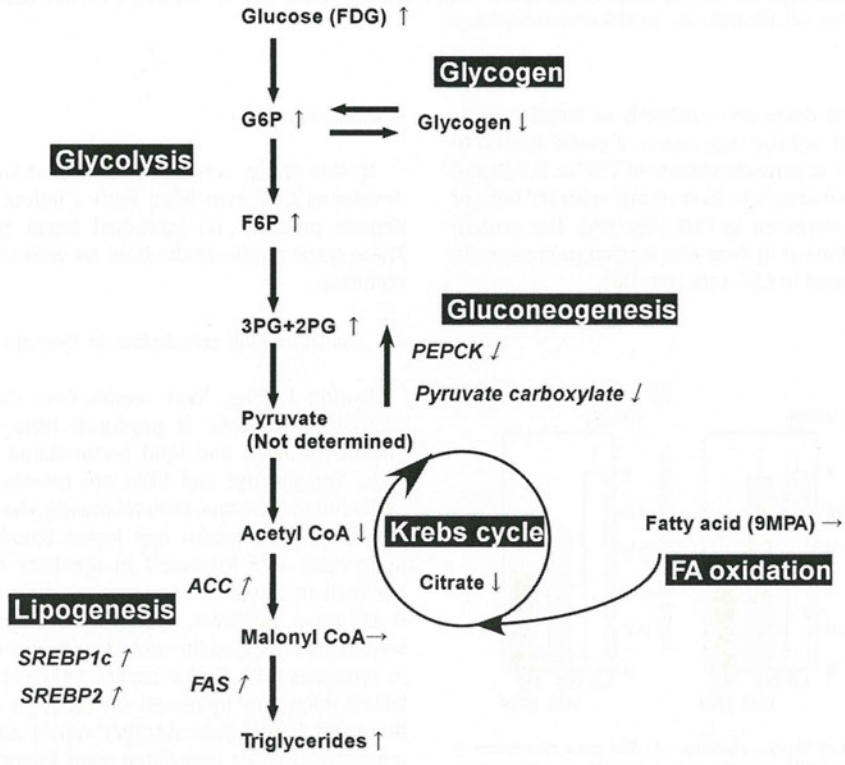

Fig. 10. Summary of the metabolic prolife in liver of CHF rats. Liver incorporated more glucose, gene expression related to gluconeogenesis was decreased, gene expression related to lipogenesis was increased, and TG content was increased in CHF rat liver.

losing weight and peripheral tissues need more substrates to maintain tissue homeostasis. Although this study is an observational one, the findings indicate the abnormal liver metabolism to be a maladaptive process and worsen the CHF. Further study of whether the modulation of liver metabolism ameliorates CHF is needed.

Acknowledgements

The authors of this manuscript have certified that they comply with the Principles of Ethical Publishing in the International Journal of Cardiology [30].

Appendix A. Supplementary data

Supplementary data to this article can be found online at doi:10.1016/j.ijcard.2011.07.056.

References

[1] Neubauer S. The failing heart — an engine out of fuel. N Engl J Med 2007;356:1140–51.
[2] Kato T, Niizuma S, Inuzuka Y, et al. Analysis of metabolic remodeling in compensated left ventricular hypertrophy and heart failure. Circ Heart Fail 2010;3:420–30.
[3] Doehner W, Rauchhaus M, Ponikowski P, et al. Impaired insulin sensitivity as an independent risk factor for mortality in patients with stable chronic heart failure. J Am Coll Cardiol 2005;46:1019–26.
[4] Anker SD, Sharma R. The syndrome of cardiac cachexia. Int J Cardiol 2002;85:51–66.
[5] Simonini A, Long CS, Dudley GA, et al. Heart failure in rats causes changes in skeletal muscle morphology and gene expression that are not explained by reduced activity. Circ Res 1996;79:128–36.
[6] Soga T, Ohashi Y, Ueno Y, Naraoka H, Tomita M, Nishioka T. Quantitative metabolome analysis using capillary electrophoresis mass spectrometry. J Proteome Res 2003;2:488–94.
[7] Rigden DJ, Jellyman AE, Frayn KN, Coppack SW. Human adipose tissue glycogen levels and responses to carbohydrate feeding. Eur J Clin Nutr 1990;44:689–92.
[8] Folch J, Lees M, Stanley GHS. A simple method for the isolation and purification of total lipids from animal tissues. J Biol Chem 1957;226:497–509.
[9] Shioi T, Kang PM, Douglas PS, et al. The conserved phosphoinositide 3-kinase pathway determines heart size in mice. EMBO J 2000;19:2537–48.
[10] Furman MP, Charney P, Mueller CM. Hepatic proteins and nutrition assessment. J Am Diet Assoc 2004;104:1258–64.
[11] Bernstein LH, Ingenbleek Y. Transthyretin: its response to malnutrition and stress injury. Clinical usefulness and economic implications. Clin Chem Lab Med 2002;40:1344–8.
[12] Inoko M, Kihara Y, Morii I, Fujiwara H, Sasayama S. Transition from compensatory hypertrophy to dilated, failing left ventricles in Dahl salt-sensitive rats. Am J Physiol 1994;267:H2471–82.
[13] Carr JG, Stevenson LW, Walden JA, Heber D. Prevalence and haemodynamic correlates of malnutrition in severe congestive heart failure secondary to ischaemic or idiopathic dilated cardiomyopathy. Am J Cardiol 1989;63:709–13.
[14] Shimano H. SREBPs: physiology and pathophysiology of the SREBP family. FEBS J 2009;276:616–21.
[15] Raghow R, Yellaturu C, Deng X, Park EA, Elam MB. SREBPs: the crossroads of physiological and pathological lipid homeostasis. Trends Endocrinol Metab 2008;19:65–73.
[16] Costa RH, Grayson DR. Site-directed mutagenesis of hepatocyte nuclear factor (HNF) binding sites in the mouse transthyretin (TTR) promoter reveal synergistic interactions with its enhancer region. Nucleic Acids Res 1991;19:4139–45.
[17] Wang Z, Burke PA. Hepatocyte nuclear factor-4α interacts with other hepatocyte nuclear factors in regulating transthyretin gene expression. FEBS J 2010;277:4066–75.
[18] Fon Tacer K, Kuzman D, Seliskar M, Pompon D, Rozman D. TNF-alpha interferes with lipid homeostasis and activates acute and proatherogenic processes. Physiol Genomics 2007;31:216–27.
[19] Sharma R, Anker SD. Cytokines, apoptosis and cachexia: the potential for TNF antagonism. Int J Cardiol 2002;85:161–71.
[20] Yndestad A, Damås JK, Oie E, Ueland T, Gullestad L, Aukrust P. Systemic inflammation in heart failure — the whys and wherefores. Heart Fail Rev 2006;11:83–92.
[21] Kleemann R, Verschuren L, van Erk MJ, et al. Atherosclerosis and liver inflammation induced by increased dietary cholesterol intake: a combined transcriptomics and metabolomics analysis. Genome Biol 2007;8:R200.
[22] Aker SD, Belosjorow S, Konietzka I, et al. Serum but not myocardial TNF-alpha concentration is increased in pacing-induced heart failure in rabbits. Am J Physiol Regul Integr Comp Physiol 2003;285:R463–9.
[23] Xie X, Liao H, Dang H, et al. Down-regulation of hepatic HNF4alpha gene expression during hyperinsulinemia via SREBPs. Mol Endocrinol 2009;23:434–43.
[24] Patel AB, de Graaf RA, Mason GF, Rothman DL, Shulman RG, Behar KL. The contribution of GABA to glutamate/glutamine cycling and energy metabolism in the rat cortex in vivo. Proc Natl Acad Sci USA 2005;102:5588–93.
[25] Metallo CM, Walther JL, Stephanopoulos G. Evaluation of ^{13}C isotopic tracers for metabolic flux analysis in mammalian cells. J Biotechnol 2009;144:167–74.
[26] Rodgers JT, Lerin C, Haas W, Gygi SP, Spiegelman BM, Puigserver P. Nutrient control of glucose homeostasis through a complex of PGC-1 and SIRT1. Nature 2005;434:113–8.
[27] Nadler EP, Dickinson EC, Beer-Stolz D, et al. Scavenging nitric oxide reduces hepatocellular injury after endotoxin challenge. Am J Physiol Gastrointest Liver Physiol 2001;281:G173–81.
[28] Puskás LG, Kitajka K, Nyakas C, Barcelo-Coblijn G, Farkas T. Short-term administration of omega 3 fatty acids from fish oil results in increased transthyretin transcription in old rat hippocampus. Proc Natl Acad Sci USA 2003;100:1580–5.
[29] Li J, Tao R, Wu W, et al. Transcriptional profiling and hepatogenic potential of acute hepatic failure-derived bone marrow mesenchymal stem cells. Differentiation 2010;80:166–74.
[30] Shewan LG, Coats AJ. Ethics in the authorship and publishing of scientific articles. Int J Cardiol 2010;144:1–2.

Metabolomics (2012) 8:624–633
DOI 10.1007/s11306-011-0353-9

ORIGINAL ARTICLE

Non-targeted metabolite profiling in activated macrophage secretion

Masahiro Sugimoto · Hiroshi Sakagami · Yoshiko Yokote · Hiromi Onuma · Miku Kaneko · Masayo Mori · Yasuko Sakaguchi · Tomoyoshi Soga · Masaru Tomita

Received: 29 March 2011 / Accepted: 9 August 2011 / Published online: 24 August 2011

Abstract Periodontal diseases are inflammatory infectious diseases that affect the periodontal tissue. Macrophages play a central role in inflammatory conditions, leading to the destruction of tissues. Identifying the signaling molecules secreted by macrophages would be valuable to the study of these diseases. Here, we present non-targeted analysis using capillary electrophoresis time-of-flight mass spectrometry (CE-TOFMS) for the profiling of extracellular metabolites released during macrophage activation. Lipopolysaccharide (LPS)-induced activation of a mouse macrophage-like cell line RAW264.7 was used as a model system. Cells were treated without (control) or with LPS for 22 h and, after washing, were incubated for 1 h in phosphate-buffered saline. The accumulation of metabolites in the culture supernatant was monitored. LPS treatment significantly enhanced the accumulation of prostaglandins, tumor necrosis factor-α, nitric oxide and citrulline in the culture medium. RAW264.7 cells produced 46 metabolites and 66% of these showed significant changes ($P < 0.05$) following cell activation. In particular, the production of leucine, hypoxanthine, choline, putrecine, N_8-acetylspermidine, succinate, itaconate, and 4-methyl-2-oxopentanoate was significantly increased by cell activation ($P < 0.001$). Significantly elevated production of lactate and glycine was also observed. Here, we present the first catalog of the up and down-regulation of the various metabolites secreted by macrophages following inflammatory activation.

Keywords Macrophage activation · Lipopolysaccharide · RAW264.7 cells · Capillary electrophoresis-mass spectrometry

1 Introduction

Periodontal disease and its milder form, gingivitis, affects 50–90% of adults worldwide, depending on the precise definition of the disease (Pihlstrom et al. 2005). The disease results in the destruction of periodontal tissues and the supporting dental structure, and is associated with systemic diseases such as diabetes, cancer, cardiovascular disease, and preterm birth (Meyer et al. 2008). Periodontal diseases are caused by complex interactions between the host tissue and bacteria at the junctional and crevicular epithelia, and is mainly mediated by the host's response to bacteria (Van Dyke and Serhan 2003).

Neutrophils and macrophages play important roles in the innate inflammatory response during the progression of periodontal disease, with sequential events being triggered by lipopolysaccharide (LPS) from gram-negative bacteria at the tooth root surface. Polymorphonuclear leukocytes are

M. Sugimoto and H. Sakagami contributed equally to this work.

M. Sugimoto (✉) · H. Onuma · M. Kaneko · M. Mori · Y. Sakaguchi · T. Soga · M. Tomita
Institute for Advanced Biosciences, Keio University, Tsuruoka, Yamagata 997-0017, Japan
e-mail: msugi@sfc.keio.ac.jp

M. Sugimoto · T. Soga · M. Tomita
Systems Biology Program, Graduate School of Media and Governance, Keio University, Fujisawa, Kanagawa 252-8520, Japan

H. Sakagami
Divisions of Pharmacology, Meikai University School of Dentistry, Sakado, Saitama 350-0283, Japan

Y. Yokote
Faculty of Science, Josai University, Sakado, Saitama 350-0295, Japan

recruited to the site, and monocytes and activated macrophages respond to endotoxin by releasing various cytokines and interleukin-1β, which stimulates further tissue destruction (Giannobile et al. 2009). Therefore, understanding the biochemical cascades induced by macrophages is important for the diagnosis and treatment of periodontal diseases.

Macrophages perform a multitude of functions essential for tissue remodeling and the immune response, and produce a wide array of pro-inflammatory cytokines, growth factors, lysozymes, proteases, complement components, coagulation factors and prostaglandins upon stimulation with LPS or hypoxic stress (Bingle et al. 2002). A mouse macrophage-like cell line (RAW264.7) (Ralph and Nakoinz 1977) has been used by many investigators in experiments designed to elucidate the signal transduction events during macrophage activation. Using this cell line, we have previously profiled amino acid release and found that the extracellular levels of glycine were significantly elevated during LPS-induced activation (Nishiyama et al. 2010). Glycine is the most abundant amino acid found in saliva (Nakamura et al. 2010) and salivary glycine levels are significantly elevated in elderly persons regardless of gender (Tanaka et al. 2010). This suggests that activated macrophages may be involved in age-related changes to salivary composition. Elevated levels of glycine in the saliva of elderly persons may aggravate periodontitis by stimulating the production of prostaglandin E_2 and cyclooxygenase-2 (COX-2) protein by interleukin-1β-stimulated human gingival fibroblast cells (Rausch-Fan et al. 2005). However, the importance of changes in glycine levels relative to other intracellular metabolite changes induced in activated macrophages remains unclear.

Metabolomics, the simultaneous quantification of all intercellular or intracellular metabolites, has become a powerful new tool that can provide insight into cellular functions (Soga et al. 2003). Several metabolites have been identified as endogenous chemical mediators that orchestrate the host's response in periodontal diseases. These metabolites include lipid-derived mediators, key inflammation signaling molecules (Van Dyke and Serhan 2003), and adenosine and inosine (Cronstein et al. 1999a, b), which are upregulated by cells in response to stress. Although the metabolite profiles of individual pathways, including lipid (Van Dyke and Serhan 2003), amino acid (Li et al. 2007) and carbohydrate (Rodriguez-Prados et al. 2010) metabolites, have been revealed, a broad understanding of these metabolomic profiles is necessary to determine the pathogenic mechanisms involved in innate macrophage inflammation in periodontal diseases.

In this study, we present the first comprehensive metabolomic analysis of the culture supernatants of unstimulated and stimulated macrophage cells to identify the metabolites secreted from macrophages at inflammatory sites such as periodontal tissues during periodontal disease. To profile a wide range of metabolites, non-targeted analyses of the extracellular environment of RAW264.7 cells treated without and with LPS were conducted using capillary electrophoresis time-of-flight mass spectrometry (CE-TOFMS) (Soga et al. 2006).

2 Materials and methods

2.1 Materials

Dulbecco's modified Eagle medium (DMEM) was purchased from GIBCO BRL (Grand Island, NY, USA), fetal bovine serum (FBS) was from JRH Biosciences (Lenexa, KS, USA) and LPS from *E. coli*, Serotype 0111:B4 was purchased from Sigma (St. Louis, MO, USA). Ophthalmate was purchased from Bachem AG (Bubendorf, Switzerland). Acetohydroxamate and azetidine-2-carboxylate were purchased from Chem Service (West Chester, PA, USA). Glucose 1-phosphate and 5-aminovalerate were purchased from Fluka (Buchs, Switzerland). Betaine was purchased from Tokyo Chemical Industry (Tokyo, Japan). All other compounds were purchased from Sigma-Aldrich (St. Louis, MO, USA) or Wako (Osaka, Japan).

2.2 Cell culture

Mouse macrophage-like RAW264.7 cells (purchased from Dainippon Sumitomo Pharma, Osaka, Japan) were cultured at 37°C in DMEM supplemented with 10% FBS under a humidified 5% CO_2 atmosphere.

2.3 LPS activation

Cells (8×10^5 cells/ml, 2 ml) were inoculated on a six-well plate (Becton–Dickinson, Labware, NJ, USA) and incubated at 37°C for 4 h for the cells to completely adhere to the plate. The medium was changed with fresh medium and the cells were then incubated for 22 h without (LPS−) or with 100 ng/ml LPS (LPS+). The experiment was carried out in triplicate. The cells were washed twice with phosphate-buffered saline without calcium or magnesium (PBS−), and then incubated in 1 mL of PBS−. An aliquot (0.5 ml) was removed immediately from each well to provide samples to analyze the initial metabolite mixture, and the cells were then incubated for 60 min at 37°C with the remaining 0.5 ml of PBS− in a 5% CO_2 incubator. All samples were centrifuged ($10{,}000 \times g$, 60 min) through a 3-kDa cutoff filter (Pall Corporation, NY, USA) to remove macromolecules, and the filtrates were assayed to detect nitric oxide (NO), tumor necrosis factor-α (TNF-α), amino acids and other cellular metabolites as described below.

A short incubation time (60 min) was used to minimize cell damage during incubation in PBS−. After incubation, the number of viable cells, which were not stained with 0.15% trypan blue in PBS−, was counted using a hemocytometer under a light microscope. The production rate for each compound was determined by subtracting the initial value from the value obtained after 60 min incubation, and expressed as nmol/10^6 cells/h.

2.4 NO assay

Since NO is a highly unstable compound, NO present in the culture medium was detected directly, without centrifugation, using the Griess method (Takahashi et al. 2008).

2.5 TNF-α assays

The culture supernatants were assayed using an ELISA kit (R&D Systems Inc, Minneapolis, MN, USA) to measure the concentration of TNF-α. The assay was performed according to the manufacturer's instructions.

2.6 Sample preparation for CE-TOFMS

To 100 μl of the extracellular-dissolved samples, 400 μl of methanol containing internal standards (50 μmol/l each of methionine sulfone, 2-[*N*-morpholino]-ethanesulfonic acid, and D-camphor-10-sulfonic acid) was added. The homogenate was then mixed with Milli-Q water and chloroform at a volume ratio of 5:2:5, and the mixture was centrifuged at 20,400×*g*, for 15 min at 4°C. The aqueous layer was filtered to remove macromolecules by centrifugation through a 5-kDa cutoff filter (Millipore) at 9,100×*g* for 2.5 h at 4°C. The filtrate (300 μl) was concentrated by centrifugation and dissolved in 50 μl of Milli-Q water containing reference compounds (200 μmol/l each of 3-aminopyrrolidine and trimesate) immediately before CE-TOFMS analysis.

2.7 Instrumental parameters for CE-TOFMS

The instrumentation and measurement conditions used for CE-TOFMS are described elsewhere (Sugimoto et al. 2010a; Soga et al. 2006, 2009). Cation analysis was performed using an Agilent CE capillary electrophoresis system, an Agilent G6220A LC/MSD TOF system, an Agilent 1100 series isocratic HPLC pump, a G1603A Agilent CE-MS adapter kit, and a G1607A Agilent CE-ESI-MS sprayer kit (Agilent Technologies, Waldbronn, Germany). Anion analysis was performed using an Agilent CE capillary electrophoresis system, an Agilent G6210A LC/MSD TOF system, an Agilent 1200 series isocratic HPLC pump, a G1603A Agilent CE-MS adapter kit and a G1607A Agilent CE-electrospray ionization (ESI) source-MS sprayer kit (Agilent Technologies). For both the cation and anion analyses, the CE-MS adapter kit includes a capillary cassette that enables thermostatic control of the capillary. The CE-ESIMS sprayer kit simplifies coupling of the CE system with the MS systems and is equipped with an electrospray source. For system control and data acquisition, we used G2201AA Agilent ChemStation software for CE and Agilent MassHunter software for TOF-MS. For anion analysis, the original Agilent SST316Ti stainless steel ESI needle was replaced with a SST316Ti stainless steel and platinum needle, which was passivated using 1% formic acid and 20% isopropanol aqueous solution at 80°C for 30 min.

For cationic metabolite analysis using CE-TOFMS (Soga et al. 2006), the samples were separated in fused silica capillaries (50 μm i.d. × 100 cm total length) filled with 1 mol/l formic acid as the reference electrolyte. Sample solutions were injected at 50 mbar for 3 s and a voltage of 30 kV was applied. The capillary temperature was maintained at 20°C and the temperature of the sample tray was kept below 5°C. The sheath liquid, composed of methanol/water (50% v/v) and 0.1 μmol/l hexakis (2,2-difluoroethoxy) phosphazene (Hexakis), was delivered at 10 μl/min. ESI-TOF-MS was conducted in the positive ion mode. The capillary voltage was set at 4 kV and the flow rate of nitrogen gas (heater temperature = 300°C) was set at 10 psig. In TOF-MS, the fragmentor, skimmer and OCT RF voltages were set at 75, 50 and 125 V, respectively. Automatic recalibration of each acquired spectrum was performed using reference masses of reference standards {[^{13}C isotopic ion of protonated methanol dimer $(2MeOH + H)]^+$, *m/z* 66.063061) and ([protonated Hexakis $(M + H)]^+$, *m/z* 622.02896}. Mass spectra were acquired at the rate of 1.5 cycles/s over a *m/z* range of 50–1,000.

For anionic metabolite analysis using CE-TOFMS (Soga et al. 2009), a commercially available COSMO(+) capillary (50 μm i.d. × 110 cm, Nacalai Tesque, Kyoto, Japan), chemically coated with a cationic polymer, was used for separation. A 50-mmol/l ammonium acetate solution (pH 8.5) was used as the electrolyte to achieve separation. Before the first use, a new capillary was flushed successively for 10 min each with the running electrolyte (pH 8.5), 50 mmol/l acetic acid (pH 3.4), and then the electrolyte again. Before each injection, the capillary was equilibrated for 2 min by flushing with 50 mM acetic acid (pH 3.4) and then for 5 min by flushing with the running electrolyte. A sample solution (30 nl) was injected at 50 mbar for 30 s, and a voltage of −30 kV was applied. The capillary temperature was maintained at 20°C and the sample tray was cooled below 5°C. An Agilent 1100 series pump equipped with a 1:100 splitter was used to deliver 5 mM ammonium acetate in 50% (v/v) methanol/water, containing 0.1 μM Hexakis to the CE interface at 10 μl/min. Here,

it was used as a sheath liquid around the outside of the CE capillary to provide a stable electrical connection between the tip of the capillary and the grounded electrospray needle. ESI-TOF-MS was conducted in negative ionization mode with the capillary voltage set to 3,500 V. For TOF-MS, the fragmentor, skimmer and Oct RF voltages were set at 100, 50 and 200 V, respectively. The flow rate of the drying nitrogen gas (heater temperature = 300°C) was 10 l/min. Automatic recalibration of each acquired spectrum was performed using reference masses of reference standards {[^{13}C isotopic ion of deprotonated acetic acid dimer (2 $CH_3COOH–H)]^-$, *m/z* 120.038339}, and {[Hexakis-deprotonated acetic acid ($CH_3COOH–H)]^-$, *m/z* 680.03554)}. Exact mass data were acquired at a rate of 1.5 spectra/s over a *m/z* range of 50–1,000.

2.8 Sample preparation for LC-TOFMS

To 30 µl of the extracellular samples, 270 µl of isopropyl alcohol containing an internal standard (2.2 µmol/l of camphor-10-sulfonic acid) was added with shaking. The mixture was centrifuged at 20,400×*g* for 10 min at 4°C, and the supernatant was then transferred to another tube and vacuum dried at 35°C. The samples were mixed with chloroform, methanol, and Milli-Q water in a volume ratio of 2:4:1 containing 20 µmol/l of 3,5-di-*tert*-butyl-4-hydroxyhydrocinnamate, centrifuged at 20,400×*g*, for 5 min at 4°C, and 25 µl of the supernatant was used for LC-TOFMS analysis.

2.9 LC-TOFMS parameters

The LC system was an Agilent 1290 infinity HPLC (Agilent Technologies). The Acquity UPLC® BEH C18 (1.7 µm), φ 2.1 × 50 mm column was purchased from Waters (Tokyo, Japan), and was maintained at 50°C. The mobile phase consisted of 0.5% acetic acid/water as eluent A and isopropanol as eluent B. A gradient of 1–99% B over 12 min was used, followed by isocratic elution at 99% for a further 17 min. The flow rate was 0.3 ml/min and the injection volume was 1 µl.

MS data were acquired on a 6530 Accurate-Mass Q-TOF LC/MS using the dual spray ESI of G-3251A (Agilent). Samples were analyzed by both positive and negative ion electrospray mass spectrometry. The MS conditions used were as follows: gas temperature 350°C, drying gas 10 l/min, nebulizer 30 psig, fragmentor 200 V, skimmer 90 V, OCT1 RF Vpp 250 V, scan range *m/z* 100–1,600 and nozzle voltage 1,000 V. The capillary voltages were 3.5 and 4.0 kV for negative and positive mode, respectively.

2.10 Determination of free amino acids

The culture medium (0.1 ml) was mixed with 0.1 ml of 10% trichloroacetic acid (Wako). After centrifugation for 5 min at 21,000×*g* at 4°C, the deproteinized supernatant was collected and stored at −30°C. The supernatants (20 µl) were analyzed using a JLC-500/V amino acid analyzer (JEOL, Tokyo, Japan) and amino acids were detected by the ninhydrin reaction (Yamazaki et al. 2007).

2.11 Data and statistical analysis

Raw data were analyzed using our proprietary software called MasterHands, which detected all possible peaks, eliminated noise and redundant features, and generated the aligned data matrix, including annotated metabolite identities and relative areas (peak areas normalized via comparison with internal standards) (Sugimoto et al. 2010b). Concentrations were calculated using external standards based on relative areas. Student's *t* test (two-tailed) was used for statistical comparisons.

3 Results and discussion

3.1 Overview of the metabolomic profiles

In total, CE-TOFMS identified 44 charged metabolites secreted by macrophages (Fig. 1; Table 1). Prostaglandin E_2 and $F_2\alpha$ were observed by LC-TOFMS as they were not charged and therefore not detected by CE-TOFMS. However, because of their similar molecular structures, these two metabolites could not be adequately resolved by LC-TOFMS, so only their combined production could be calculated and used in subsequent analyses.

3.2 Validation of the amino acid profiles determined by CE-TOFMS and the amino acid analyzer

The quantified amino acids were validated by comparing the amino acids profiles consistently obtained by CE-TOFMS with those obtained using an amino acid analyzer (Fig. 2). The metabolites present at high concentrations, such as glycine, alanine and threonine, showed slightly greater discrepancy between the profiles determined by the two methods than metabolites present at low concentrations. Nevertheless, reasonably high overall correlation coefficients were obtained for the unstimulated and LPS-stimulated macrophages, which were $R = 0.855$ ($P < 0.0001$, Pearson correlation) and $R = 0.928$ ($P < 0.0001$, Pearson correlation), respectively.

3.3 Stimulatory effect of LPS on macrophages

NO production by stimulated RAW264.7 cells was significantly increased from 0.20 to 0.66 nmol/10^6 cells/h (3.3-fold increase, $P = 0.0002$) (Fig. 3a), and TNF-α production was also significantly increased from 21.7 to 682.5 pg/10^6 cells/h

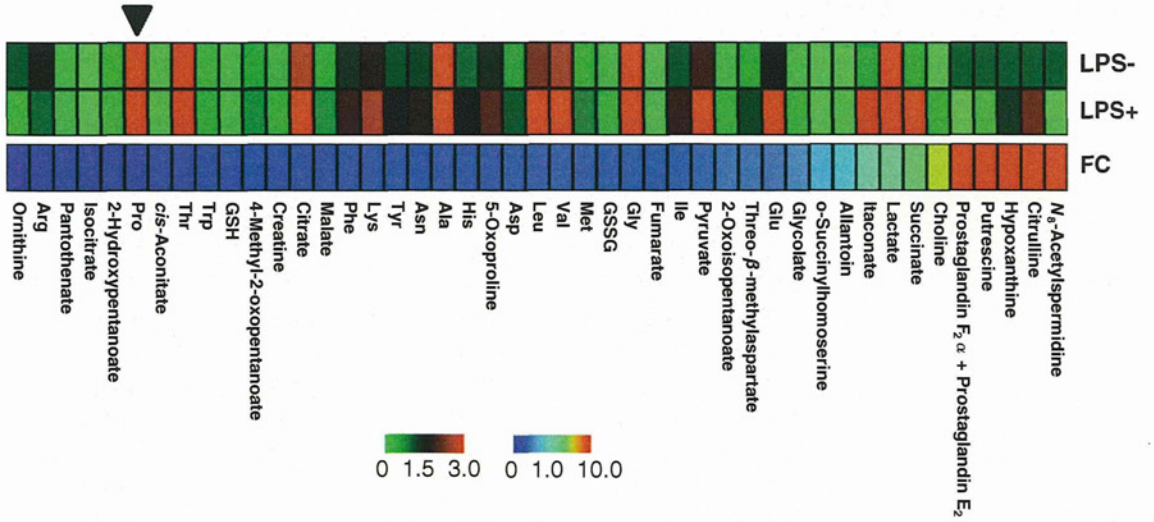

Fig. 1 *Heatmap* and *bar graph* visualization of the quantified metabolites. *Heatmap* showing the quantified metabolites using a *green–black–red scheme*, and the fold-change of metabolites in LPS+ versus LPS− cells. Where metabolites were not detected in LPS− cells, a 10-fold change was allocated. Proline, marked with *triangle*, showed no change. *FC* fold change

(31.5-fold increase, $P = 0.0151$) (Fig. 3b). Citrulline production, which accompanies NO production at a molar ratio of 1:1, is generated from arginine by inducible NO synthase (Paradise et al. 2010). It was only observed for stimulated RAW264.7 cells (2.19 nmol/10^6 cells/h, $P = 3.0 \times 10^{-5}$) (Table 1). Since NO is labile, citrulline levels are a more reliable guide to the levels of NO synthase activity. These data confirmed that LPS activated the RAW264.7 cells.

Prostaglandin E_2 and $F_2\alpha$, detected by LC-TOFMS, are central molecules in inflammatory processes. The inflammatory response of macrophages induces prostanoid synthesis by (1) inducing mobilization of the fatty acid substrate arachidonate from membrane phospholipids, (2) promoting prostaglandin H_2 production from arachidonate by upregulating cyclooxygenases 1 and 2 (COX-1/2), and (3) converting prostaglandin H_2 to specific prostanoids, such as prostaglandin E_2 and $F_2\alpha$ (Noguchi and Ishikawa 2007). The production of prostaglandin E_2 and $F_2\alpha$ (4.6×10^{-3} nmol/10^6 cells/h, $P = 1.2 \times 10^{-6}$) was only observed in stimulated RAW264.7 cells, again confirming the activation of these macrophages.

3.4 Amino acid profiles of stimulated macrophages

3.4.1 Glycine, serine and cysteine production

In amino acid profiles, glycine production was the highest of all amino acids detected (LPS− vs. LPS+: 17.1 vs. 29.5 nmol/10^6 cells/h, $P = 0.073$) (Table 1), which is consistent with previous studies using LPS-stimulated mouse macrophages and regular culture medium (DMEM + 10% FBS) (Nishiyama et al. 2010). Glycine has been reported to stimulate the production of prostaglandin E_2 and COX-2 protein in interleukin-1β-stimulated human gingival fibroblast cells, suggesting its involvement in the pathogenesis of periodontitis (Rausch-Fan et al. 2005). On the other hand, glycine has been reported to inhibit the production of inflammatory cytokines by macrophages by blocking calcium channels (Rose et al. 1999), inhibiting TNF-α secretion and increasing IL-10 production (Xu et al. 2008), or via neutral amino acid transporters (Carmans et al. 2010). Glycine inhibited the growth of an endothelial cell line (Yamashina et al. 2007) and salivary gland-derived progenitor cells (Nakamura et al. 2009). Although these data are contradictory, they mostly suggest that glycine negatively regulates the growth and activation of various cultured cells. This metabolite is also the most abundant amino acid in the saliva (Takeda et al. 2009; Tanaka et al. 2010); however, the cells in the oral cavity that secrete glycine have not been identified. In association with glycine pathway, serine, a major source of glycine, was only detected by the amino acid analyzer, but was present at relatively low concentrations (Table 1; LPS− vs. LPS+: 1.0 ± 0.074 vs. 1.1 ± 0.12 nmol/10^6 cells/h, 1.1 fold). Cysteine, which is synthesized from serine, was not observed, possibly due to the limited supply of serine.

3.4.2 Glutamate, glutamine, proline and arginine production

Glutamate, a key intermediate in amino acid metabolism, including biosynthetic and degradative pathways, is formed from α-ketoglutarate in the tricarboxylic acid (TCA) cycle. We found that glutamate production was increased by 2.2-fold ($P = 0.0043$) in activated macrophages, and its

Table 1 Profiled metabolites of RAW264.7 cells

Mode	Metabolite	LPS−		LPS+		*P* value	FC
		Mean	SD	Mean	SD		
C	Gly	17.1	7.79	29.4	4.21	0.0735	1.7
C	Ala	8.61	1.65	13.1	3.19	0.0988	1.5
C	Thr	7.50	0.594	9.13	0.501	0.0219	1.2
C	Pro	4.17	0.385	4.22	0.323	0.891	1.0
C	Val	2.50	0.424	4.18	0.361	6.41×10^{-3}	1.7
C	Leu	2.25	0.227	3.75	0.153	6.80×10^{-4}	1.7
C	Glu	1.48	0.0657	3.28	0.530	4.31×10^{-3}	2.2
C	Lys	1.72	0.231	2.54	0.337	0.0251	1.5
C	Cit	0.00	0.00	2.19	0.180	3.01×10^{-5}	N.A
C	Ile	1.04	0.232	1.86	0.0675	4.19×10^{-3}	1.8
C	Phe	1.27	0.180	1.86	0.182	0.0162	1.5
C	Asn	1.14	0.194	1.72	0.222	0.0275	1.5
C	Tyr	1.07	0.182	1.61	0.101	0.0111	1.5
C	His	0.970	0.0954	1.48	0.186	0.0134	1.5
C	Asp	0.630	0.119	1.03	0.477	0.235	1.6
C	Arg	1.62	0.196	0.958	0.0862	6.01×10^{-3}	0.59
C	Met	0.482	0.160	0.822	0.0944	0.0340	1.7
C	Trp	0.334	0.0286	0.446	0.0218	5.81×10^{-3}	1.3
C	Hypoxanthine	0.00	0.00	1.22	0.0797	1.21×10^{-5}	N.A.
C	5-Oxoproline	1.34	0.213	2.05	0.310	0.0311	1.5
C	Choline	0.0554	2.52×10^{-3}	0.408	0.0101	5.13×10^{-7}	7.4
C	Creatine	0.287	0.0418	0.401	0.0696	0.0715	1.4
C	Ornithine	1.04	0.239	0.383	0.109	0.0123	0.37
C	Putrescine	0.00	0.00	0.315	0.0605	8.36×10^{-4}	N.A.
C	Allantoin	0.0342	0.415	0.129	2.41	0.950	3.8
C	*o*-Succinylhomoserine	0.0142	0.0480	0.0475	0.0318	0.373	3.3
C	N_8-Acetylspermidine	0.00	0.00	0.0277	2.52×10^{-3}	4.55×10^{-5}	N.A.
C	GSSG	0.217	0.0323	0.371	0.0667	0.0225	1.7
C	GSH	0.118	0.0233	0.164	0.0883	0.428	1.4
A	Glycolate	0.142	0.935	0.367	0.240	0.359	2.6
A	Pyruvate	1.91	0.958	3.66	0.632	9.38×10^{-3}	1.9
A	Lactate	6.65	3.36	37.0	7.58	2.33×10^{-3}	5.6
A	Fumarate	0.0676	0.110	0.117	0.0289	0.291	1.7
A	2-Oxoisopentanoate	0.171	0.238	0.370	0.0370	0.0875	2.2
A	Succinate	0.513	0.237	3.16	0.400	3.30×10^{-4}	6.2
A	2-Hydroxypentanoate	0.379	0.198	0.328	0.0575	0.525	0.86
A	Itaconate	0.549	0.269	2.86	0.254	1.18×10^{-4}	5.2
A	4-Methyl-2-oxopentanoate	0.509	0.256	0.711	0.0391	4.20×10^{-3}	1.4
A	Malate	0.479	0.243	0.680	0.0800	0.0363	1.4
A	Threo-β-methylaspartate	0.511	0.286	1.13	0.0967	1.33×10^{-3}	2.2
A	*cis*-Aconitate	0.114	0.0579	0.123	0.0154	0.562	1.1
A	Isocitrate	0.0520	1.31	0.0444	0.0386	0.761	0.85
A	Citrate	2.62	1.32	3.69	0.485	0.0357	1.4
A	Pantothenate	0.240	0.121	0.184	0.0315	0.0818	0.77

Table 1 continued

Mode	Metabolite	LPS−		LPS+		*P* value	FC
		Mean	SD	Mean	SD		
N	Prostaglandin $F_2\alpha$+ Prostaglandin E_2	0.00	0.00	4.62×10^{-3}	1.68×10^{-4}	1.16×10^{-6}	N.A.

Units are nmol/10^6 cells/h. The metabolite concentraton in LPS− cells was 0 nmol/10^6 cells/h

SD standard deviation; *FC* fold-change; *C* cationic; *A* anionic; *N* neutral; *NA* not applicable

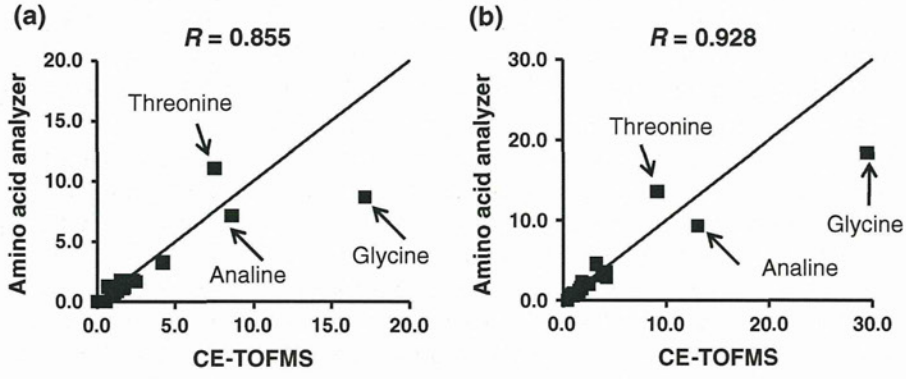

Fig. 2 Comparison of amino acid productions determined by CE-TOFMS and the amino acid analyzer for LPS− (**a**) and LPS+ macrophages (**b**). Units for both *X*- and *Y*-axis are nmol/10^6 cells/h

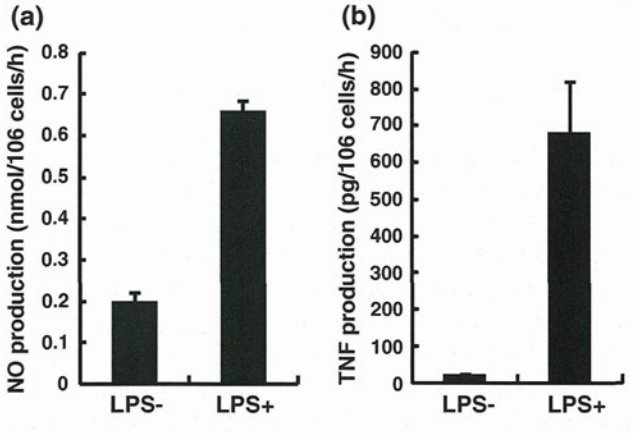

Fig. 3 Stimulation of NO (**a**) and TNF-α (**b**) production in LPS-activated RAW264.7 cells. Values are means ± standard deviation of triplicate determinations

fold-change in production was the highest observed for any amino acid. Glutamate is an excitatory neurotransmitter and the glutamate receptor protein is present on the macrophage cell surface (Noda et al. 2000). Glutamate plays a number of roles in the immune system including removal of oxidants and regulation of immune response (Li et al. 2007). Increased glutamate production in LPS-activated macrophages has already been reported (Stuckey et al. 2005). Glutamate is also a substrate in the synthesis of γ-aminobutyrate (GABA), present in macrophages (Stuckey et al. 2005). However, in this study, GABA was not detected in the culture supernatant of the activated macrophages.

Proline is synthesized from glutamate, but its concentration did not change, despite LPS stimulation (1.0-fold, $P = 0.891$). In contrast, significant decreases in arginine (0.59-fold, $P = 6.01 \times 10^{-3}$) and ornithine (0.37-fold, $P = 0.109$) were observed; ornithine is synthesized from arginine by arginase. Considering the excessive increase of citrulline upon macrophage activation, the arginine pathway seems to be highly activated and mainly used for citrulline synthesis,

3.4.3 Production of other amino acids

The production of alanine (1.5-fold, $P = 0.0988$), valine (1.7-fold, $P = 6.41 \times 10^{-3}$), and leucine (1.7-fold, $P = 6.80 \times 10^{-4}$) was increased to a similar extent by macrophage activation. The production of pyruvate, their precursor metabolite, was also elevated (1.9-fold, $P = 9.38 \times 10^{-3}$). Thus, the change of these metabolites might be due to pyruvate elevation. Aspartate (1.6-fold), which is formed from the TCA component oxaloacetate by the action of transaminase, and its downstream metabolites such as asparagine, lysine, methionine, threonine, isoleucine (from 1.2 to 1.8-fold), showed similar upregulation (Fig. 4; Table 1). On the other hand, cysteine was undetected, probably because of its degradation during sample preparation before CE-TOFMS.

3.5 Metabolomic profile of carbohydrate metabolism

3.5.1 Lactate production

Lactate production in activated macrophages was significantly elevated, and this elevation was the largest observed of all metabolites (37.0 nmol/10^6 cells/h, 5.57-fold increase, $P = 0.0023$). This finding is consistent with previous reports showing that glycolysis and lactate production were increased during osteoclast differentiation induced by receptor activator of nuclear factor [NB]-κB ligand (RANKL) in RAW264.7 cells (Kim et al. 2007). The increase in lactate production, the end product of mono-oxidative glycolysis, indicates that the glycolysis pathway is activated. Enhanced glycolysis in macrophages is likely to be a survival strategy to cope with the low oxygen conditions commonly observed at inflammatory lesions (Roiniotis et al. 2009). Lactate is a signaling molecule that can activate macrophages by stimulating inflammatory pathways, such as the TLR4 and NF-κB pathways (Samuvel et al. 2009; Nareika et al. 2005). Combined stimulation with LPS and lactate was shown to enhance macrophage activation more than LPS alone (Samuvel et al. 2009). The positive correlation between lactate production and macrophage activation observed here suggests an interaction between extracellular lactate and macrophages, possibly by a feed-forward loop, although further studies are necessary to confirm this postulation.

3.5.2 The balance between glycolysis and TCA cycle activation

Although less substantial than the change in lactate production, a significant increase in TCA cycle metabolite production was observed following macrophage activation. The levels of citrate, succinate, itaconate, malate and fumarate all increased following activation (Table 1). Rodriguez-Prados et al. (2010) observed upregulation of genes involved in glycolysis and downregulation of genes involved in the TCA cycle of LPS-activated macrophages. Indeed, the production of pyruvate in our study was significantly increased (1.9-fold, $P = 0.0094$). It is plausible that glycolysis was activated in activated macrophages under conditions where overall energy metabolism was enhanced. This implies that, even though genes in the TCA cycle were downregulated, the excessive activation of glycolysis caused a slight increase in several metabolites of the TCA cycle.

3.6 Oxidative stress

Barnes et al. (2009) found that the levels of hypoxanthine, inosine, xanthine, guanosine and guanine in gingival crevicular fluid (GCF) were elevated in inflammation sites compared with healthy sites in a human oral cavity. Their findings suggest accelerated activity of the purine degradation pathway and the production of reactive oxygen species causing marked cellular oxidative stress. In this study, we only detected hypoxanthine in activated macrophages (1.22 nmol/10^6 cells/h, $P = 1.2 \times 10^{-5}$).

GSH plays an anti-inflammatory role via its role as an antioxidant (Ghezzi 2011). The production of GSH was increased slightly (1.4-fold, $P = 0.43$), while the production of GSSG was significantly increased after activation in this study (1.7-fold, $P = 0.022$). The ratio of GSH and GSSG decreased slightly from 0.54 to 0.44 ($P = 0.64$) but this decrease was at levels below those considered significant, indicating no dramatic change in oxidative stress after treating macrophages with LPS. Allantoin, which is a uric acid oxidation product, and is therefore a marker for oxidative stress (Kand'ar et al. 2006), also showed no significant changes following exposure to LPS (3.8-fold, $P = 0.95$). These findings conflict with the elevated production of hypoxanthine, a marker for oxidative stress. Therefore, the profiling of cellular metabolites and integration of those data with the extracellular profiles determined in this study would be valuable.

3.7 Other metabolites secreted by macrophages

In addition to amino acids and metabolites related to energy metabolism, several other metabolites were also identified. The production of threo-β-methylaspartate, which is generated from oxaloacetate and NH_3 via threo-3-hydroxy-L-aspartate ammonia-lyase, was significantly increased following activation (2.2-fold, $P = 0.0013$). N_8-Acetylspermidine ($P = 4.5 \times 10^{-5}$, not detected in LPS− cells), a polyamine that generally indicates active cell growth, was only detected in activated macrophages. While the increases following activation were statistically significant ($P > 0.05$) for the following metabolites, there

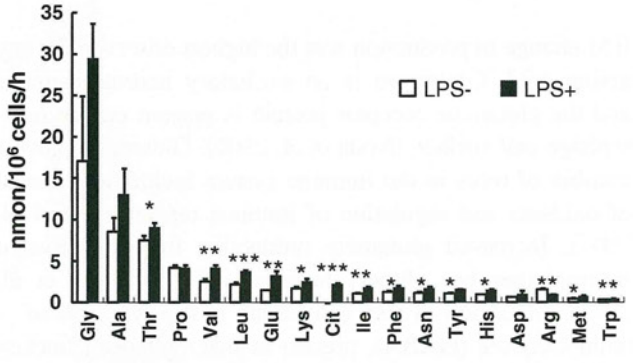

Fig. 4 *Bar graph* showing amino acid production profiles in LPS+ and LPS− cells. Values are means ± standard deviation. $*P < 0.05$, $**P < 0.01$ and $***P < 0.001$

were small increases in the production of *o*-succinylhomoserine, glyconate and 2-oxoisopentanoate, which showed high fold-changes compared with most amino acids (>1.7-fold) (Table 1). The biological relevance of these metabolites should be confirmed using other "-omics" data and cellular metabolite profiles.

4 Concluding remarks

In this study, we conducted CE-TOFMS-based metabolomics analysis to identify the metabolites secreted by LPS-stimulated macrophage-like RAW264.7 cells. Cellular activation was confirmed by the increased production of NO, citrulline, TNF-α and prostaglandins E_2 and $F_2\alpha$ by the stimulated cells. In addition to large increases in glycine production, the production of lactate was also enhanced, indicating the activation of glycolysis. Increased production of several intermediates in the TCA cycle was also observed. Of oxidative stress-related metabolites, the production of hypoxanthine was particularly high, although the GSSH/GSH ratio was almost unchanged by LPS stimulation. To understand these conflicting results, studies using integrated cellular metabolomics profiles are needed to elucidate how the observed metabolite changes contribute to the subsequent inflammatory events in periodontal disease. Nevertheless, this report provides the first catalog of the various metabolites secreted by activated macrophages, and complements prior reports on the already well-studied pro-inflammatory proteins that are known to be secreted by macrophages.

Acknowledgments This work was supported by research funds from the Yamagata Prefectural Government and the city of Tsuruoka. We thank Shinobu Abe for technical assistance.

Conflicts of interest The authors have no conflicts of interest to declare.

References

Barnes, V. M., Teles, R., Trivedi, H. M., Devizio, W., Xu, T., Mitchell, M. W., et al. (2009). Acceleration of purine degradation by periodontal diseases. *Journal of Dental Research, 88*(9), 851–855.

Bingle, L., Brown, N. J., & Lewis, C. E. (2002). The role of tumour-associated macrophages in tumour progression: Implications for new anticancer therapies. *Journal of Pathology, 196*(3), 254–265.

Carmans, S., Hendriks, J. J., Thewissen, K., Van den Eynden, J., Stinissen, P., Rigo, J. M., et al. (2010). The inhibitory neurotransmitter glycine modulates macrophage activity by activation of neutral amino acid transporters. *Journal of Neuroscience Research, 88*(11), 2420–2430.

Cronstein, B. N., Montesinos, M. C., & Weissmann, G. (1999a). Salicylates and sulfasalazine, but not glucocorticoids, inhibit leukocyte accumulation by an adenosine-dependent mechanism that is independent of inhibition of prostaglandin synthesis and p105 of NFkappaB. *Proceedings of the National Academy of Sciences of the United States of America, 96*(11), 6377–6381.

Cronstein, B. N., Montesinos, M. C., & Weissmann, G. (1999b). Sites of action for future therapy: An adenosine-dependent mechanism by which aspirin retains its antiinflammatory activity in cyclooxygenase-2 and NFkappaB knockout mice. *Osteoarthritis and Cartilage, 7*(4), 361–363.

Ghezzi, P. (2011). Role of glutathione in immunity and inflammation in the lung. *International Journal of General Medicine, 4*, 105–113.

Giannobile, W. V., Beikler, T., Kinney, J. S., Ramseier, C. A., Morelli, T., & Wong, D. T. (2009). Saliva as a diagnostic tool for periodontal disease: Current state and future directions. *Periodontology, 2000*(50), 52–64.

Kand'ar, R., Zakova, P., & Muzakova, V. (2006). Monitoring of antioxidant properties of uric acid in humans for a consideration measuring of levels of allantoin in plasma by liquid chromatography. *Clinica Chimica Acta, 365*(1–2), 249–256.

Kim, J. M., Jeong, D., Kang, H. K., Jung, S. Y., Kang, S. S., & Min, B. M. (2007). Osteoclast precursors display dynamic metabolic shifts toward accelerated glucose metabolism at an early stage of RANKL-stimulated osteoclast differentiation. *Cellular Physiology and Biochemistry, 20*(6), 935–946.

Li, P., Yin, Y. L., Li, D., Woo Kim, S., & Wu, G. (2007). Amino acids and immune function. *British Journal of Nutrition, 98*(02), 237–252.

Meyer, M. S., Joshipura, K., Giovannucci, E., & Michaud, D. S. (2008). A review of the relationship between tooth loss, periodontal disease, and cancer. *Cancer Causes and Control, 19*(9), 895–907.

Nakamura, Y., Kodama, H., Satoh, T., Adachi, K., Watanabe, S., Yokote, Y., et al. (2010). Diurnal changes in salivary amino acid concentrations. *In Vivo, 24*(6), 837–842.

Nakamura, Y., Matsumoto, S., Mochida, T., Nakamura, K., Takehana, K., & Endo, F. (2009). Glycine regulates proliferation and differentiation of salivary-gland-derived progenitor cells. *Cell and Tissue Research, 336*(2), 203–212.

Nareika, A., He, L., Game, B. A., Slate, E. H., Sanders, J. J., London, S. D., et al. (2005). Sodium lactate increases LPS-stimulated MMP and cytokine expression in U937 histiocytes by enhancing AP-1 and NF-kappaB transcriptional activities. *American Journal of Physiology—Endocrinology and Metabolism, 289*(4), E534–E542.

Nishiyama, A., Yokote, Y., & Sakagami, H. (2010). Changes in amino acid metabolism during activation of mouse macrophage-like cell lines. *In Vivo, 24*(6), 857–860.

Noda, M., Nakanishi, H., Nabekura, J., & Akaike, N. (2000). AMPA-kainate subtypes of glutamate receptor in rat cerebral microglia. *The Journal of Neuroscience, 20*(1), 251.

Noguchi, K., & Ishikawa, I. (2007). The roles of cyclooxygenase-2 and prostaglandin E_2 in periodontal disease. *Periodontology, 2000*(43), 85–101.

Paradise, W. A., Vesper, B. J., Goel, A., et al. (2010). Nitric oxide: Perspectives and emerging studies of a well known cytotoxin. *International Journal of Molecular Sciences, 11*, 2715–2745.

Pihlstrom, B. L., Michalowicz, B. S., & Johnson, N. W. (2005). Periodontal diseases. *The Lancet, 366*(9499), 1809–1820.

Ralph, P., & Nakoinz, I. (1977). Antibody-dependent killing of erythrocyte and tumor targets by macrophage-related cell lines: Enhancement by PPD and LPS. *Journal of Immunology, 119*(3), 950–954.

Rausch-Fan, X., Ulm, C., Jensen-Jarolim, E., Schedle, A., Boltz-Nitulescu, G., Rausch, W. D., et al. (2005). Interleukin-1beta-induced prostaglandin E_2 production by human gingival fibroblasts is upregulated by glycine. *Journal of Periodontology, 76*(7), 1182–1188.

Rodriguez-Prados, J. C., Traves, P. G., Cuenca, J., Rico, D., Aragones, J., Martin-Sanz, P., et al. (2010). Substrate fate in activated macrophages: A comparison between innate, classic, and alternative activation. *Journal of Immunology, 185*(1), 605–614.

Roiniotis, J., Dinh, H., Masendycz, P., Turner, A., Elsegood, C. L., Scholz, G. M., et al. (2009). Hypoxia prolongs monocyte/macrophage survival and enhanced glycolysis is associated with their maturation under aerobic conditions. *Journal of Immunology, 182*(12), 7974–7981.

Rose, M. L., Rivera, C. A., Bradford, B. U., Graves, L. M., Cattley, R. C., Schoonhoven, R., et al. (1999). Kupffer cell oxidant production is central to the mechanism of peroxisome proliferators. *Carcinogenesis, 20*(1), 27–33.

Samuvel, D. J., Sundararaj, K. P., Nareika, A., Lopes-Virella, M. F., & Huang, Y. (2009). Lactate boosts TLR4 signaling and NF-kappaB pathway-mediated gene transcription in macrophages via monocarboxylate transporters and MD-2 up-regulation. *Journal of Immunology, 182*(4), 2476–2484.

Soga, T., Baran, R., Suematsu, M., Ueno, Y., Ikeda, S., Sakurakawa, T., et al. (2006). Differential metabolomics reveals ophthalmic acid as an oxidative stress biomarker indicating hepatic glutathione consumption. *Journal of Biological Chemistry, 281*(24), 16768–16776.

Soga, T., Igarashi, K., Ito, C., Mizobuchi, K., Zimmermann, H. P., & Tomita, M. (2009). Metabolomic profiling of anionic metabolites by capillary electrophoresis mass spectrometry. *Analytical Chemistry, 81*(15), 6165–6174.

Soga, T., Ohashi, Y., Ueno, Y., Naraoka, H., Tomita, M., & Nishioka, T. (2003). Quantitative metabolome analysis using capillary electrophoresis mass spectrometry. *Journal of Proteome Research, 2*(5), 488–494.

Stuckey, D., Anthony, D., Lowe, J., Miller, J., Palm, W., Styles, P., et al. (2005). Detection of the inhibitory neurotransmitter GABA in macrophages by magnetic resonance spectroscopy. *Journal of Leukocyte Biology, 78*(2), 393.

Sugimoto, M., Goto, H., Otomo, K., Ito, M., Onuma, H., Suzuki, A., et al. (2010a). Metabolomic profiles and sensory attributes of edamame under various storage duration and temperature conditions. *Journal of Agriculture and Food Chemistry, 58*(14), 8418–8425.

Sugimoto, M., Wong, D. T., Hirayama, A., Soga, T., & Tomita, M. (2010b). Capillary electrophoresis mass spectrometry-based saliva metabolomics identified oral, breast and pancreatic cancer-specific profiles. *Metabolomics, 6*(1), 78–95.

Takahashi, J., Sekine, T., Nishishiro, M., Arai, A., Wakabayashi, H., Kurihara, T., et al. (2008). Inhibition of NO production in LPS-stimulated mouse macrophage-like cells by trihaloacetylazulene derivatives. *Anticancer Research, 28*(1A), 171–178.

Takeda, I., Stretch, C., Barnaby, P., Bhatnager, K., Rankin, K., Fu, H., et al. (2009). Understanding the human salivary metabolome. *NMR in Biomedicine, 22*(6), 577–584.

Tanaka, S., Machino, M., Akita, S., Yokote, Y., & Sakagami, H. (2010). Changes in salivary amino acid composition during aging. *In Vivo, 24*(6), 853–856.

Van Dyke, T. E., & Serhan, C. N. (2003). Resolution of inflammation: A new paradigm for the pathogenesis of periodontal diseases. *Journal of Dental Research, 82*(2), 82–90.

Xu, F. L., You, H. B., Li, X. H., Chen, X. F., Liu, Z. J., & Gong, J. P. (2008). Glycine attenuates endotoxin-induced liver injury by downregulating TLR4 signaling in Kupffer cells. *American Journal of Surgery, 196*(1), 139–148.

Yamashina, S., Ikejima, K., Rusyn, I., & Sato, N. (2007). Glycine as a potent anti-angiogenic nutrient for tumor growth. *Journal of Gastroenterology and Hepatology, 22*(Suppl 1), S62–S64.

Yamazaki, T., Yamazaki, A., Onuki, H., Hibino, Y., Yokote, Y., Sakagami, H., et al. (2007). Effect of saliva, epigallocatechin gallate and hypoxia on Cu-induced oxidation and cytotoxicity. *In Vivo, 21*(4), 603–607.

メタボロミクスによるがんの診断マーカー探索

曽　我　朋　義

メタボロミクスは，細胞や組織に存在する代謝産物の変化を，バイアスをかけない方法論で包括的に探索する手法であり，近年，幅広い研究分野に用いられるようになってきた．ここでは，疾患診断マーカー探索への応用を概説する．

メタボロミクスとは

細胞は，外界から取入れたグルコースなどの栄養源を酵素反応によってさまざまな物質に変換（代謝）し，活動するために必要な物質群を産生している．この代謝産物の総称はメタボロームとよばれ，分子量が1000以下の低分子化合物である．メタボロームの種類は生物種によって異なり，大腸菌などの微生物は数百，哺乳動物は数千，植物は数万種類が存在する．

メタボローム解析はメタボロミクスとよばれ，代謝物を大規模に測定し，代謝や細胞の働きを包括的に理解しようとする方法論である．代謝制御機構，酵素やトランスポーターの機能解明のみならず，代謝異常やがんなどの機序解明，バイオマーカー探索，疾病診断，創薬，工業用微生物の開発など，最近では幅広い分野にメタボローム解析が応

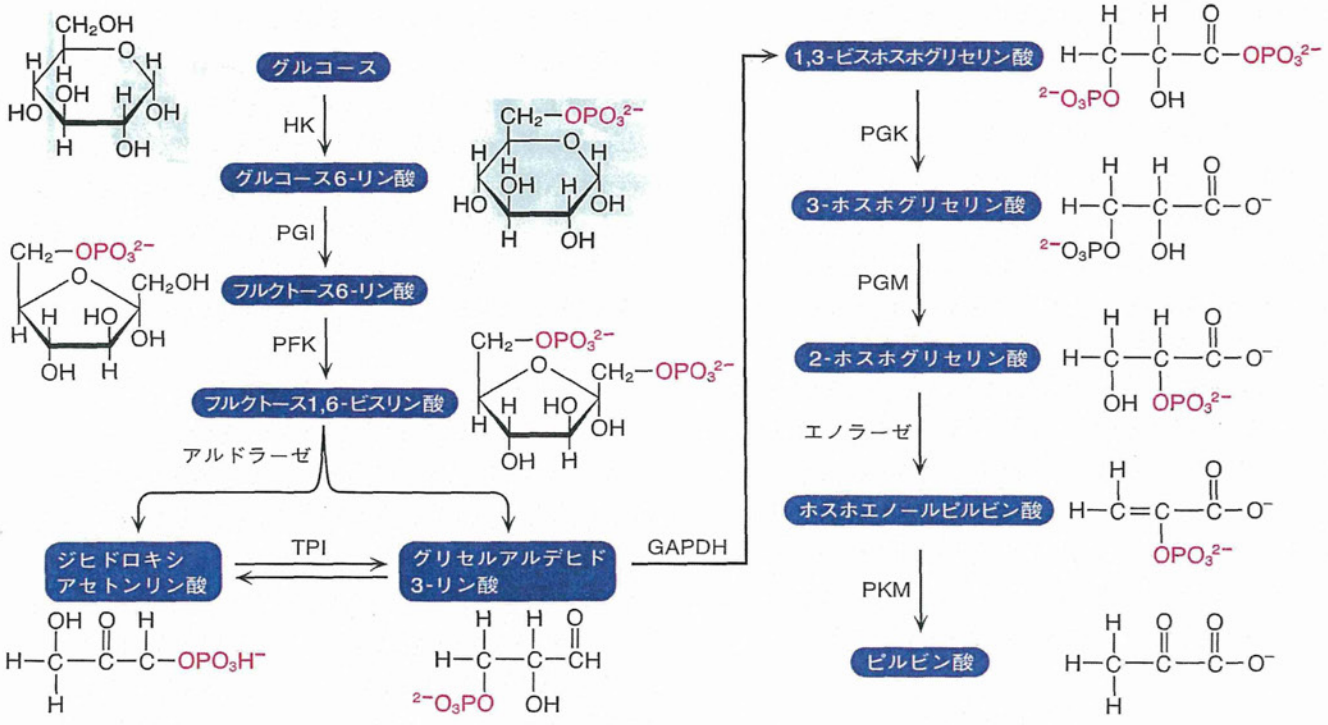

赤はリン酸基を示す．解糖系の前半の代謝物は糖にリン酸基，後半の代謝物はカルボン酸にリン酸基が結合しておりイオン性が高い．

図1　解糖系の代謝中間体の構造